

## Cenozoic biostratigraphy of larger foraminifera from equatorial carbonate platform of northwestern Brazil

Dayana Alvarado Sierra<sup>a</sup>, Orangel Aguilera<sup>b,\*</sup>, Olga M. Oliveira de Araújo<sup>c</sup>, Ricardo Tadeu Lopes<sup>c</sup>, Mauro Geraldés<sup>d</sup>, Maria Virginia Alves Martins<sup>d,e</sup>, Giovanni Coletti<sup>f</sup>, Beatriz Teixeira Guimarães<sup>a</sup>, Ana Paula Linhares<sup>g</sup>, Vinicius Tavares Kütter<sup>a</sup>

<sup>a</sup> Federal University of Pará, Geoscience Institute, Augusto Correa, n°1, CEP 66075-110, Belém, Pará, Brazil

<sup>b</sup> Fluminense Federal University, Paleocology and Global Changes Laboratory, Rua Marcos Waldemar de Freitas Reis, s/ n°, Campus Gragoatá, Bloco M, Lab. 110, CEP 24210-201, Niterói, Rio de Janeiro, Brazil

<sup>c</sup> Federal University of Rio de Janeiro, Nuclear Instrumentation Laboratory, Nuclear Engineering Program/COPPE, Rio de Janeiro, Av. Horácio Macedo, Cidade Universitária, CEP 21941-450, Brazil

<sup>d</sup> Rio de Janeiro State University, Geology Faculty, Av. São Francisco Xavier, 524, Lab-4037F, Maracanã. CEP 20550-013, Rio de Janeiro, Brazil

<sup>e</sup> Aveiro University, GeoBioTEC Research Unity, Campus de Santiago, Aveiro, Portugal

<sup>f</sup> University of Milano Bicocca, Department of Environmental Sciences and Earth Sciences, Piazza della Scienza 4, 20126 Milano, Italy

<sup>g</sup> Museu Paraense Emílio Goeldi, Earth Sciences and Ecology Coordination, CEP 66077-830, Belém, Pará, Brazil

### ARTICLE INFO

#### Keywords:

Ilha de Santana Formation  
Rupelian–Burdigalian  
Foraminifera  
Micro-CT  
Petrography  
South America

### ABSTRACT

The off-shore Cenozoic succession of the Pará–Maranhão Basin of the Brazilian equatorial margin is studied to investigate skeletal and foraminiferal assemblages during the Oligocene–Miocene interval, one of the fundamental moments in the environmental evolution of our planet. The material from core 1-MAS-16-MA is analyzed using a combination of conventional paleontological analyses, and innovative approaches like micro-CT scan and U/Pb dating on carbonates. The results allowed to clearly constrain the Oligocene – Miocene interval and divide it into four foraminiferal assemblages and seven biofacies useful for both paleoenvironmental reconstructions and stratigraphic correlations. The paleoenvironmental analysis indicates a common pattern of relative sea-level oscillations with the nearby Foz do Amazonas Basin, highlighting a common behavior of this part of the equatorial passive margin during the Oligocene – Miocene interval. The comparison between the succession of skeletal and foraminiferal assemblages of the investigated core and other successions of the Southern and Central American area indicated the presence of stratigraphically relevant foraminiferal assemblages that could be useful for improving the correlation between the various Cenozoic successions of the area (assemblages dominated by nummulitids and lepidocyclinids in the Rupelian; assemblages dominated by *Heterostegina (Vlerkina) antillea*, lepidocyclinids, and primitive miogypsinids in the Chattian; assemblages dominated by *Heterostegina (Vlerkina) antillea*, lepidocyclinids, and miogypsinids other than *Miogypsinoides* and *Miogypsinella*, in the Aquitanian; assemblages dominated by advanced miogypsinids in the Burdigalian; post Early Miocene assemblages characterized by the lack of abundant lepidocyclinids and miogypsinids). Finally, the overall resilience of most of the large benthic foraminifera taxa to the Oligocene – Miocene transition testifies once more to the adaptability of this group of carbonate producers.

### 1. Introduction

During the Cenozoic, Earth's climate shifted from the greenhouse conditions of the early Paleogene to the icehouse conditions of the late

Neogene. A key moment of this transition is represented by the Oligocene and Miocene epochs. During the early Oligocene, following the opening of the Drake Passage and the isolation of Antarctica from other landmass, a remarkable drop in temperature is suggested by the stable

\* Corresponding author.

E-mail addresses: [dayana.sierra@ig.ufpa.br](mailto:dayana.sierra@ig.ufpa.br) (D. Alvarado Sierra), [orangelaaguilera@id.uff.br](mailto:orangelaaguilera@id.uff.br) (O. Aguilera), [olgaufjrjlin@gmail.com](mailto:olgaufjrjlin@gmail.com) (O.M. Oliveira de Araújo), [ricardo@lin.ufrj.br](mailto:ricardo@lin.ufrj.br) (R.T. Lopes), [mauro.geraldes@gmail.com](mailto:mauro.geraldes@gmail.com) (M. Geraldés), [virginia.martins@ua.pt](mailto:virginia.martins@ua.pt) (M.V. Alves Martins), [giovanni.p.m.coletti@gmail.com](mailto:giovanni.p.m.coletti@gmail.com) (G. Coletti), [beatriz.97.guimaraes@gmail.com](mailto:beatriz.97.guimaraes@gmail.com) (B.T. Guimarães), [alinhares@museu-goeldi.br](mailto:alinhares@museu-goeldi.br) (A.P. Linhares), [viniciuskutter@id.uff.br](mailto:viniciuskutter@id.uff.br) (V.T. Kütter).

<https://doi.org/10.1016/j.marpetgeo.2023.106458>

Received 13 May 2023; Received in revised form 7 August 2023; Accepted 10 August 2023

Available online 12 August 2023

0264-8172/© 2023 Elsevier Ltd. All rights reserved.

isotopes record of deep-sea benthic foraminifera and is correlated with the development of ice-sheets in Antarctica (Zachos et al., 2001; Lagabriele et al., 2009; Miller et al., 2020). During the Oligocene – Early Miocene interval, these masses of continental ice were relatively unstable and characterized by major periods of growth and decay corresponding to sea-level variations of c. 40–60 m (Miller et al., 2020). These waxing and waning episodes were relatively rapid and, similarly to Pleistocene glacial-interglacial cycles, characterized by both orbital and CO<sub>2</sub> forcing (Greenop et al., 2019). These events are also recorded in shallow marine benthic assemblage by important groups of carbonate producers such as colonial corals, red calcareous algae, and large benthic foraminifera (Perrin and Bosellini, 2012; Pomar et al., 2017; Boudagher-Fadel, 2018; Coletti et al., 2022). However, given the patchy and discontinuous nature of the geological record of continental shelves, the global response of shallow-water environments to the climatic oscillations of the Oligocene-Early Miocene interval is still poorly understood.

Currently the equatorial Brazilian shelf is characterized by mixed carbonate-siliciclastic deposits (Testa and Bosence, 1999; De Mahiques et al., 2019) whose bioclastic fraction is largely consisting of heterozoan carbonates (*sensu* James, 1997; Michel et al., 2018). Carbonate production is dominated by red calcareous algae and mainly occur off-shore, far away from the mouth of major rivers, resulting in an extensive and economically relevant ecosystems (Coletti et al., 2017; De Mahiques et al., 2019). These sedimentary deposits represent only the uppermost portion of the thick Cenozoic sedimentary sequence of the Brazilian passive margin (Cruz et al., 2019) that includes several subsurface units, namely the Amapá Formation (Foz do Amazonas Basin: Schaller et al., 1971), the Ilha de Santana Formation (Pará-Maranhão Basin: Abreu et al., 1986; Brandão and Feijó, 1994; Soares et al., 2007), the Pirabas Formation (recorded in the Barreirinhas Basin: Pamplona, 1969; Trostdorf Jr. et al., 2007), and the Guamaré Formation (Ceará Basin: Condé et al., 2007; Potiguar Basin: Pessoa Neto et al., 2007) (Fig. 1). Some of the basin in which the margin is subdivided, namely the Potiguar, Ceará, and Pará-Maranhão basins, are known for having potentially significant hydrocarbon systems, with some of the aforementioned

Cenozoic formations acting as reservoirs (Pellegrini and Ribeiro, 2018). On the other hand, no significant production has been achieved (yet) in the Foz do Amazonas, Pará-Maranhão, and Barreirinhas basins (Pellegrini and Ribeiro, 2018). These basins constitute the natural uninterrupted continuation of Guyana–Suriname–French Guiana equatorial margin (Zalán et al., 2019). Recent discoveries of multiple active petroleum systems in this northwestern area sparked further interest into the Foz do Amazonas and Pará-Maranhão basins (Pellegrini and Ribeiro, 2018; D’Almeida et al., 2019).

For the purpose of hydrocarbon exploration core 1-MAS-16-MA was drilled in the Pará-Maranhão Basin. The analysis of the core led to the recognition of the Ilha de Santana Formation within the Humberto de Campos Group (Abreu et al., 1986; Brandão and Feijó, 1994; Soares et al., 2007; Zalán, 2015; Pellegrini and Ribeiro, 2018). The Ilha de Santana Formation comprises an extensive carbonate package that spans most of the Cenozoic and consists of i) calcarenites and calcirudites, deposited in the inner platform; ii) calcarenites and calcilitutes, deposited in the middle platform; and iii) marls, shales, and mudstones, deposited in the outer platform and along the slope (Figueiredo et al., 2007; Brandão and Feijó, 1994). Currently there are no accurate micropaleontological and geochronological data on the Ilha de Santana Formation, nor data on the skeletal assemblages of the bioclastic intervals. An unpublished master’s thesis recorded the foraminifera and radiolarians of Cretaceous age from the interval comprised between 3552 and 4290 m below sea floor (mbsf from here onward) (Da Silva, 2007).

In order to improve our knowledge on the environmentally crucial Oligocene – Early Miocene interval in an otherwise poorly investigated area and to provide more data to correlate the different formations that constitute the sedimentary succession of the Brazilian equatorial margin, we here examine samples of the Ilha de Santana Formation from core 1-MAS-16-MA corresponding to a depth interval that should include the Oligocene – Miocene transition (Fig. 1). Samples are analyzed with an innovative approach based on the combination of micro-computed tomography (micro-CT), optical microscope and scanning electron microscope, focusing on the foraminiferal assemblages

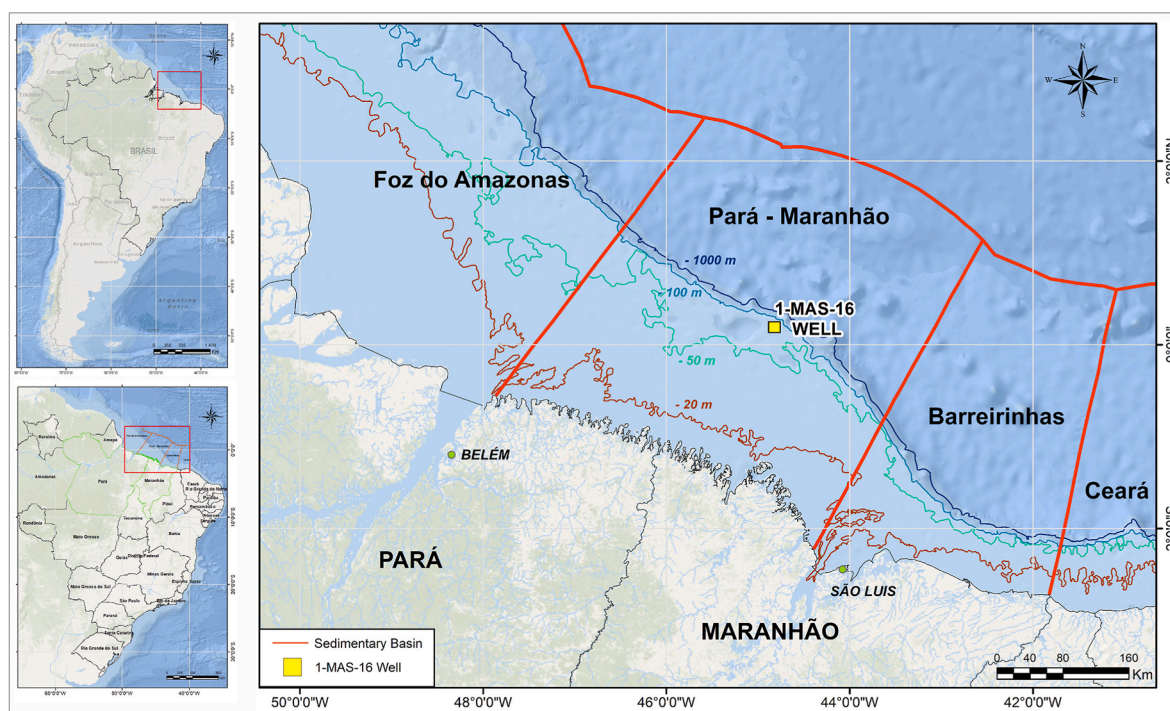


**Fig. 1.** Map of the northwestern equatorial basins of Brazil, highlighting the Pará-Maranhão Basin and the reference location of the PETROBRAS well 1-MAS-16-MA (0° 14' 9.30" N; 44° 48' 21.25" W).

and in particular on large benthic foraminifera (LBF from here onward) that can provide useful insights for both biostratigraphy and paleo-environmental reconstructions. Further data are also provided on the skeletal assemblage. The investigated sedimentary succession is then correlated with the other coeval succession of the Foz do Amazonas Basin (de Mello e Souza, 1994; de Mello e Sousa et al., 2003; Cruz et al., 2019) and Campos Basin (BouDagher-Fadel et al., 2010). The studied succession is also compared and correlated with the uppermost portion of the Pirabas Formation exposed along the coast of the Pará state and that represents the youngest bioclastic unit of the succession of the Pará-Maranhão Basin (Aguilera et al., 2020a;b; Aguilera et al., 2022). The results of this research will elucidate the distribution of several groups of LBF as well as the evolution of South American carbonate systems during the Oligocene – Early Miocene interval.

2. Materials and methods

The material from the core 1-MAS-16-MA from the Pará-Maranhão Basin (Fig. 1), and the associated data of the well drill (ANP Protocol 48610.211469/2019–39), were loaned by the Brazilian National Petroleum Agency (ANP, Protocol SAA 46.19), to be analyzed at the Paleocology and Global Changes Laboratory at Federal Fluminense University. Only gutter samples (cuttings) were available from the core. Given the intrinsic uncertainty related to the stratigraphic placement of gutter samples as well as the scarcity of available material, it was decided to perform highly detailed analyses on a selected amount of samples chosen with a large spacing, within the core succession. A total

of 42 gutter samples (cuttings) was then collected from the strata between 500 and 1200 mbsf. Based on the existing preliminary data from drilling operations, this interval should have comprised the Oligocene – Miocene transition. The samples were randomly selected each 20 m interval, then quartered and divided into 9 g sub-samples to pick benthic foraminifera under the stereo microscope. LBF were selected for studying the detailed external morphology using the scanning electronic microscope (SEM). These selected specimens were mounted on aluminum supports with a diameter of 12 mm using double-sided carbon adhesive tape, gold-plated for over 90 s creating a film with an average thickness of 12 nm. The images were generated by secondary electron detection using a voltage acceleration between 5 and 1 kV and a working distance of approximately 15 mm. Given the value of internal structures for the identification of LBF, on selected well-preserved specimens micro-CT acquisitions of picked specimens were also performed (Phoenix v|tome|x M 300; Baker Hughes, Wunstorf, Germany). To create the 3D models, slice alignment, beam hardening correction, and ring artifact reduction were implemented with Phoenix Data. A mathematical edge-enhancement filter was applied to achieve a higher contrast. For model visualization, VG Studio Max v 3.0 was used. LBF identification follows: Loeblich and Tappan (1988), Banner and Hodgkinson (1991), BouDagher-Fadel and Price (2010a, b), BouDagher-Fadel (2018), Coletti et al. (2018), de Mello e Sousa et al. (2003, 2009), and Mitchell et al. (2022). Species level identifications were based on biometric analyses performed on the equatorial plane of well-preserved specimens (Fig. 2).

To have a better grasp of both skeletal and foraminiferal

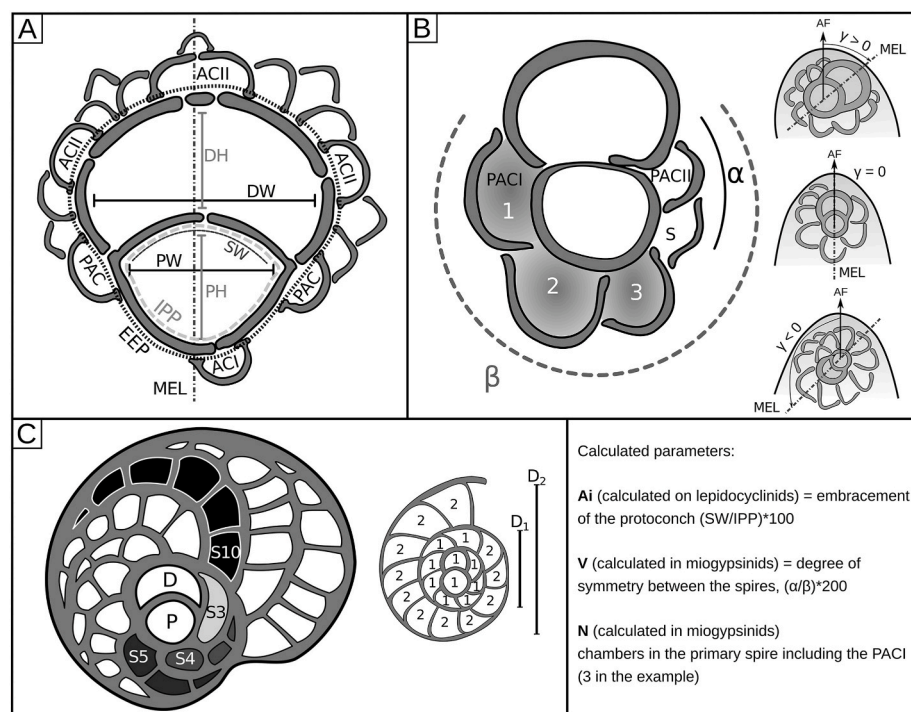


**Fig. 2.** Biometric parameters in megalospheric specimens of lepidocyclinids, miogypsinids, and heterostegins, modified from Coletti et al. (2019). A) Schematic view of the embryonic apparatus of a lepidocyclinid viewed on the equatorial plane; modified from Van Vessem (1978); MEL = medio embryonic line, i.e. the line passing through the centers of the protoconch and the deuteroconch; PW = width of the protoconch excluding wall thickness, measured perpendicular to the MEL; PH = height of the protoconch, excluding wall thickness, measured along the MEL; PL = height of the protoconch, excluding wall thickness, measured in the axial plane along a direction perpendicular to the equatorial plane (not visible in the figure); DW = width of the deuteroconch measured perpendicular to the MEL; DH = height of the deuteroconch measured along the MEL; IPP = internal perimeter of the protoconch; SW = length of the shared wall between the protoconch and the deuteroconch; NACII = numbers of auxiliary chambers of the deuteroconch (ACII); EPP = external perimeter of the embryo composed of protoconch and deuteroconch. B) Schematic view of the embryonic apparatus of a miogypsinid, modified from De Bock (1973); Özcan et al., (2009); PACI = first principal auxiliary chambers, from which the primary nepionic spire (numbered grey chambers) start; S = symmetric chamber marking the end of the secondary nepionic spire. X = number of chambers in the primary nepionic spire (numbered grey chambers in the example). PACII = second principal auxiliary chamber (usually smaller than PACI), from which the secondary nepionic spire starts (constituted only by the

PACII in the example);  $\alpha$  = radial sector of the protoconch (expressed in degrees) directly covered by the secondary nepionic spire;  $\beta$  = radial sector (expressed in degrees) of the protoconch directly covered by either the primary or the secondary nepionic spire; AF = line that connects the upper most part (apex) of the frontal portion of the test to the center of the protoconch;  $\gamma$  = the angle (expressed in degrees) between the AF and the MEL,  $\gamma$  is positive when the deuteroconch is directed toward the apex, but negative when it faces in the opposite direction or when the primary nepionic spire is longer than one whorl. C) Schematic view of the embryonic apparatus of a heterostegind and of a coiled foraminifer; modified from Coletti et al., (2018). P = protoconch; D = deuteroconch; OC = number of undivided (operculind) post-embryonic chambers, one in the example; SX = number of chamberlets in the Xth chamber; D1 = diameter of the 1st whorl; D2 = diameter of the 2nd whorl; NC1 = number of chambers in the 1st whorl (which are marked by 1 in the example); NC2 = number of chambers in the 2nd whorl (which are marked by 2 in the example).

assemblages, pristine subsamples (i.e., those sub-samples in which benthic foraminifera were not collected by picking) were also analyzed. One set of sub-samples was used for the preparation of thin sections. The material was embedded in epoxy resins and then fixed on  $76 \times 26$  mm glass slides and polished to a thickness of  $30 \mu\text{m}$ . Photomicrographs were obtained using a petrographic microscope equipped with an integrated digital system. Another set of pristine subsamples was used for further micro-CT scan acquisitions. Subsamples were placed in Eppendorf vials (1.5 ml), and then the scanning was performed using the Phoenix v|tome|x M 300. Phoenix Data software was used for creating the 3D models, while the analysis of the models was performed using AVIZO. Foraminiferal taxonomy was investigated, rotating the 3D models of the Eppendorf vials until the desired internal morphometric feature of the specimen was fully visible. The composition of the foraminiferal assemblage was then calculated averaging the data from picking analyses, dedicated micro-CT scans and SEM analyses with data from the observation of the 3D models of pristine samples. Data were then statistically treated by hierarchical cluster analysis based on the Bray-Curtis similarity with PRIMER 6 (Kruskal, 1977; Field et al., 1982; Clarke and Gorley, 2006). Since data on foraminifera abundance were assembled from different sources a semi-quantitative scale was employed for reporting and a comparison: dominant >50%; 50% > commonly present >10%; 10% > moderately present >2%; 2% > rarely present. One every two samples was analyzed for skeletal assemblage composition. Each slice composing the 3D model on the XY plane was investigated, recognizing all the identifiable skeletal grains based on their internal structure. The analysis was then repeated for each slice composing the model on the YZ plane. Data on skeletal assemblage composition for the XY and YZ planes were then combined. Given the inherent uncertain of combining the two datasets, the data were then organized and reported using the semi-quantitative scale proposed by Carey et al. (1995) for modern skeletal assemblages: 0% = absent; 1% > very rare >0%; 5% > rare >1%; 10% > non rare >5%; 25% > common >10%; 50% > abundant >25%; dominant >50%.

The implementation of the U–Pb method for geochronology was based on the analytical protocols of Roberts et al. (2020) and Cardoso et al. (2023). We used a Thermo Fisher Element 2 ICP-MS coupled to a Photon Machines Analyte Excite ArF 193 nm excimer laser ablation system for the analyses. The operative conditions were: RF power of 1200 W; ablation time of 40 s; fluency  $<5 \text{ J/cm}^2$ ; spot size  $150 \mu\text{m}$ , and repetition rate of 10 Hz. NIST 612 was used to normalize the 207 Pb/206 Pb ratios, while the carbonate reference material WC-1 (Roberts et al., 2017) was used for 206 Pb/238U corrections based on the WC-1 age obtained in the same analytical session. The samples to be analyzed were selected according to the abundance of the main foraminifera genera and each 100 m of depth of the core. A total of five samples of benthic foraminifera and one sample of coralline algae were analyzed, and for each sample 4 to 6 subsamples were selected. The specimens were organized in the same horizontal plane, embedded in acrylic resin on a circular mold, dried, and polished to a thickness of test surface exposures. These samples were randomly screened to assess their viability to be dated, with the help of the SEM's map images. Regions with U counts  $<10,000$  cps were discarded. After delimiting promising regions within these six samples, the analyses sessions took place and was performed in sequential rounds, each round consisting of 25 spots. In total 390 spots (including five spots on the NIST 612 standard) were analyzed in each round, 5 of which were NIST 612 analyses, 15 analyses of samples (benthic foraminifera), and 5 analyses of WC-1. Data reduction was done using the softwares Glitter (Griffin et al., 2008) and SATURNO. After reduction, data were plotted in Tera-Wasserburg diagrams, and lower intercept ages were calculated with IsoplotR (Vermeesch, 2021). Final ages were calculated after eliminating outliers.

### 3. Results

#### 3.1. Skeletal assemblages

Micro-CT scan analysis of the cuttings embedded in Eppendorf vials highlighted the presence of seven different biofacies (BF-1 to BF-7) dominated by red calcareous algae (mainly crustose but also articulated taxa) and LBF (Fig. 3) (Table 1). Encrusting benthic foraminifera, small benthic foraminifera, and bryozoans can be locally relevant. Molluscs, echinoderms, corals, and *Halimeda* are usually rare. A qualitative examination under the stereomicroscope of the samples suggest that ostracods, echinoderms, decapod crustaceans, and fish remain also occur, but they are always rare.

The first biofacies (BF-1; 510–650 mbsf) is dominated by fragments of red calcareous algae (RCA) and LBF, mainly amphisteginids but also minor amounts of soritids. Other relevant components are small benthic foraminifera (both hyaline and porcelaneous). Encrusting benthic foraminifera, molluscs, bryozoans, corals, *Halimeda*, and echinoderms are rare.

BF-2 (660–798 mbsf) is dominated by RCA and miogypsinids. Amphisteginids are also a common component. Bryozoans are relevant towards the lower part of the interval. Encrusting benthic foraminifera, molluscs, echinoderms, corals, and *Halimeda* are rare.

BF-3 (805–918 mbsf) is dominated by RCA, miogypsinids, and lepidocyclinids. Bryozoans are another common component, while molluscs, echinoderms, and encrusting benthic foraminifera are rare.

BF-4 can be observed in a narrow interval close to 950 mbsf and is characterized by the dominance of RCA, miogypsinids and lepidocyclinids, associated with common heterosteginids (mainly *Heterostegina (Vlerkina) antillea*). Bryozoans are also present but not as common as in BF-3. Encrusting benthic foraminifera (mainly *Victoriella*), molluscs and small benthic foraminifera are rare.

BF-5 (950–1050 mbsf) is dominated by RCA and a diversified LBF assemblage that includes heterosteginids (mainly *Heterostegina (Vlerkina) antillea*), lepidocyclinids, and miogypsinids. Encrusting benthic foraminifera (mainly *Victoriella*) are a common component. Molluscs and bryozoans are rare.

BF-6 (1050–1165 mbsf) is dominated by RCA and nummulitids, among them *Heterostegina* is still present but not as common as in the previous biofacies. Lepidocyclinids and small benthic foraminifera are common, while encrusting benthic foraminifera (mainly *Victoriella*), molluscs, bryozoans, and echinoderms are rare.

BF-7 (1200) can be observed at the bottom of the studied interval and is dominated by RCA associated with common lepidocyclinids and encrusting benthic foraminifera (commonly represented by *Victoriella*). Small benthic foraminifera, molluscs, and echinoderms are rare.

#### 3.2. Foraminiferal assemblages

Of the 42 samples analyzed, four groups of LBF are most abundant and dominate the assemblages in most of sample: amphisteginids, miogypsinids, lepidocyclinids, and heterosteginids (Table 2). *Sphaerogypsina* and *Victoriella* are relatively common but never dominant, while the remaining taxa are rare. Using Bray-Curtis similarity on the raw foraminiferal data, it was possible to recognize four clusters corresponding to four foraminiferal assemblages (IS-1 to IS-4) (Fig. 4).

IS-1 characterizes the calcarenites of the upper-part of the studied interval of the core (510–660 mbsf). This assemblage is dominated by small benthic foraminifera and LBF. Among these, *Amphistegina* (Figs. 5 and 6) and *Sphaerogypsina* (Figs. 5 and 7) are the most common. Planorbulinids (Figs. 7 and 8), *Victoriella* (Figs. 5 and 6), *Textularia* (Fig. 7), *Pyrgo* (Figs. 7 and 8), *Archaias* (Figs. 7 and 8), *Sorites* (Figs. 7 and 8), *Quinqueloculina* (Fig. 7) also occur.

IS-2 can be recognized in the samples related to the calcarenites and calcilitites of the interval comprised between 660 and 798 mbsf. It is characterized by the dominance of miogypsinids (Fig. 9) and

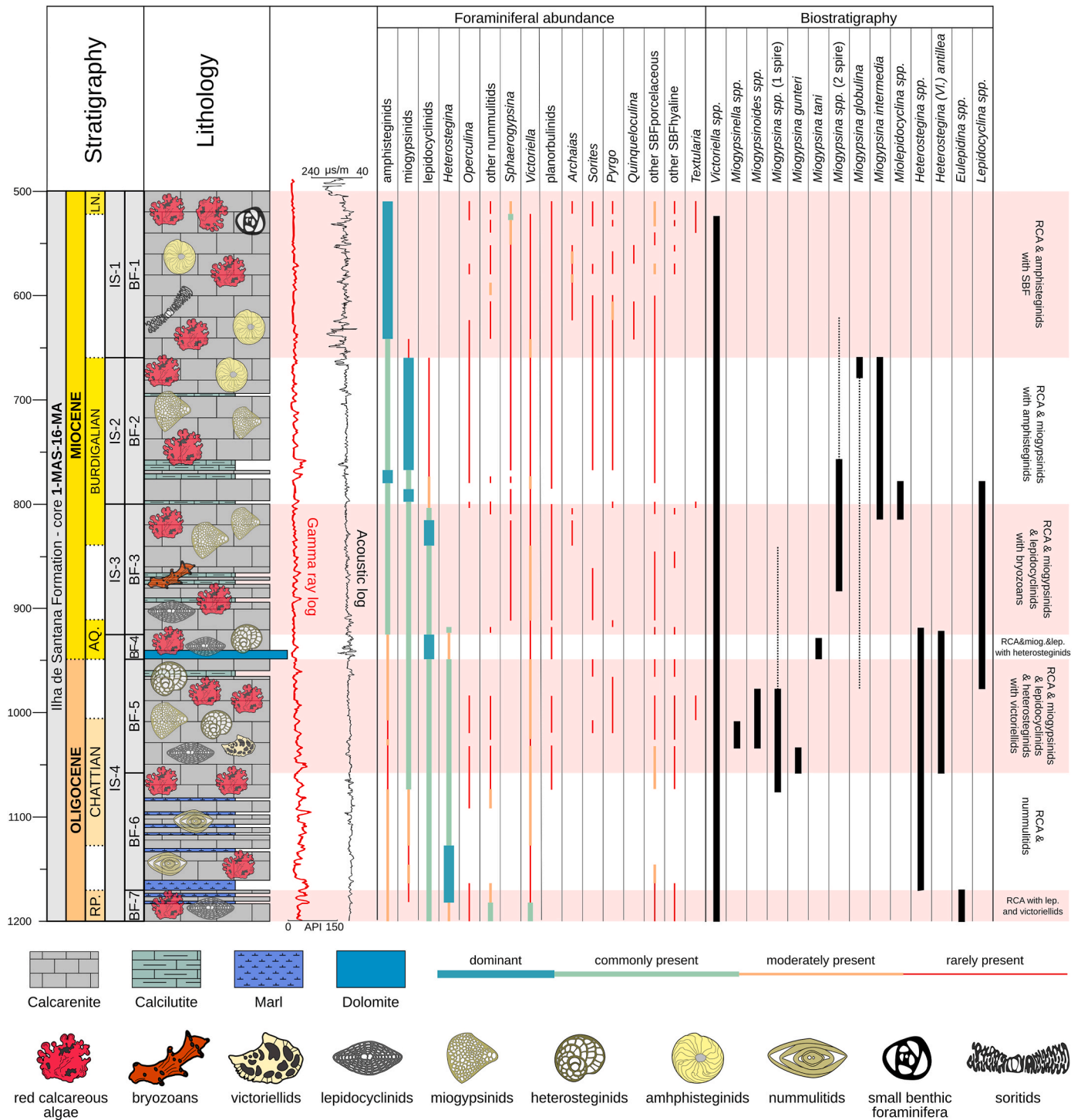


Fig. 3. Schematic section of the Ilha de Santana Formation from the PETROBRAS well section 1-MAS-16-MA, showing the age intervals, lithology, analyzed samples at section, abundance of the main groups of foraminifera and occurrences of age diagnostic taxa, biofacies and skeletal components, gamma ray, and sonic profile. The data used for lithology and gamma-ray and sonic logs were taken from the wells drill data (Brazilian National Petroleum Agency Protocol 48610.211469/2019–39). RP = Rupelian; AQ = Aquitanian; LN = Langhian; RCA = red calcareous algae; SBF = small benthic foraminifera; Vl. = *Vlerkina*.

amphisteginids. *Lepidocyclinids* (Fig. 10), *planorbulind*s, *Victoriella*, *Sphaerogypsina*, *Textularia*, *Pyrgo* and other small benthic foraminifera are rare.

IS-3 characterizes the calcarenites interbedded with calcilutites of the intermediate portion of the studied interval of core 1-MAS-16-MA (805–948 mbsf). It is dominated by *lepidocyclinids*, associated with common (and locally very common) *miogypsinids* and *amphisteginids*. *Victoriella* is moderately common, while *planorbulind*s and

*Sphaerogypsina* are rare or absent.

IS-4 assemblage can be recognized in the interval comprised between 950 mbsf and the lower limit of the investigated interval of the core (1200 mbsf). It is dominated by *heterosteginids*, associated with common *lepidocyclinids* and *Victoriella* (Figs. 8 and 9). Locally, various other *nummulitids* and *Amphistegina* can be moderately common. *Miogypsinids* and *Operculina* are rare.

**Table 1**  
Skeletal assemblage composition from the Ilha de Santana Formation in the PETROBRAS well 1-MAS-16-MA at section from 510 to 1200 mbsf; the implemented semi-quantitative scale follows Carey et al. (1995); 1%> very rare (vr)>0%; 5%>non rare (nr)>1%; 10%>non rare (nr)>5%; 25%>common (c)>10%; 50%>abundant (A)>25%; dominant (D)>50%; other acronyms are as follows: LBF= large benthic foraminifera; EBF= encrusting benthic foraminifera; SBF= small benthic foraminifera; RCA= red calcareous algae; MOL= molluscs; BRY= bryozoans; ECH= echinoderms; HAL= Halimeda; COR= corals.

	510	525	528	570	624	624	642	660	768	774	798	805	846	858	918	948	984	1008	1020	1032	1074	1164	1200	
amphisteginids																								
miogypsinids & lepidocyclinids	A	D	A	D	C	C	C	nr	C	C	A	nr	F	nr	F	F	F	vr	vr	vr	vr	vr	vr	vr
nummulitids	vr	A	A	A	A	A	A	A	A	A	A	A	C	C	C	C	C	C						
other LBF hyaline	nr	nr	nr	nr	vr	vr	vr	vr	vr	vr	vr													
LBF porcellanaceous	F	F	F	F	vr	vr	vr	vr	vr	vr	vr													
EBF																								
SBF	C	C	C	C	F	F	F	F	F	F	F	F	nr	vr	vr	vr	vr	vr	vr	vr	vr	vr	vr	vr
RCA	F	C	A	C	D	D	D	A	A	A	A	A	A	A	A	A	A	A	A	A	A	A	A	A
MOL	nr	nr	F	F	nr	nr	nr	F	F	F	F	F	F	F	F	F	F	F	F	F	F	F	F	F
BRY	F	F	F	F	vr	vr	vr	F	F	F	F	F	F	F	F	F	F	F	F	F	F	F	F	F
ECH	F	F	F	F	F	F	F	F	F	F	F	F	F	F	F	F	F	F	F	F	F	F	F	F
HAL																								
COR	nr	vr	vr	F	F	F	F	nr	nr	vr	vr	vr	vr	vr	vr	vr								
Other				vr	vr	vr	vr	vr	vr	vr														

3.3. Biostratigraphy

Micro-CT scan analysis, supported by thin sections, allowed for the identification of several age diagnostic taxa of LBF within the investigated section of the core. *Victoriella* occurs in most of the samples (510–1200 mbsf); according to BouDagher-Fadel (2018) this genus ranges from the late Eocene to the Early Miocene. *Miogypsinella* has been identified in samples at 1008 and 1032 mbsf and, according to BouDagher-Fadel and Price (2010a) analysis of American miogypsinids, spans from the late Rupelian to the Chattian. The genus *Miogypsinoides* has been recognized in samples at 984, 1008, and 1020 mbsf and, based on BouDagher-Fadel and Price (2010a), should be restricted to the late Rupelian. However, in the Mediterranean and Indo-Pacific area is known to be mainly restricted to the Chattian stage (Cahuzac and Poignant, 1997; Dill et al., 2020). *Miogypsin* species characterized by a single long spire are common in the interval comprised between 984 and 1074 mbsf and rare between 846 and 984 mbsf. In particular *Miogypsin gunteri*, which is characterized by a long spire, has been identified in samples from 1026 to 1032 mbsf. *Miogypsin tani*, which is characterized by a shorter spire in comparison to *M. gunteri*, has been instead recognized in a sample at 948 mbsf. According to BouDagher-Fadel and Price (2010a) *M. gunteri* ranges from the late Rupelian to the Chattian while *M. tani* goes from the latest Rupelian to the Aquitanian. *Miogypsin* species with multiple spires have been recognized in samples from 624 to 966 mbsf, but most of clearly identifiable specimens occur between 660 and 858 mbsf. In particular, *Miogypsin globulina* has been recognized between 660 and 966 mbsf, and *Miogypsin intermedia* between 660 and 805 mbsf. Based on BouDagher-Fadel and Price (2010a) both species extend from the Chattian to the Burdigalian. On the other hand, according to Robinson (2004) the genus *Miogypsin*, in the Caribbean, is mainly restricted to the Early Miocene and, based on Butterlin (1981, 1987) *Miogypsin intermedia* should extend from the Burdigalian to the Langhian. The genus *Mirolepidocyclina* has been recognized in samples from 774 to 805 mbsf; this genus, according to BouDagher-Fadel and Price (2010a), extends from the latest Rupelian to the Burdigalian. *Heterostegina (Vlerkina)* has been recognized between 918 and 1164 mbsf, while the species *Heterostegina (Vlerkina) antillea*, has been recognized between 924 and 1032 mbsf. More rare and poorly preserved heterosteginids were also observed at 1200 mbsf. According to BouDagher-Fadel et al. (2010), *H. antillea* should occur between the late Rupelian and the early Chattian, while, according to Robinson (2004) it should extend from the Chattian to the Aquitanian. The genus *Eulepidina*, mainly represented by fragmented individuals, have been recognized in samples from 1164 to 1200 mbsf. Based on Robinson (2004) and Mitchell et al. (2022), *Eulepidina* ranges from the Priabonian to the Aquitanian, while for BouDagher-Fadel et al. (2010) it extends also into the Burdigalian. Different species of *Lepidocyclina* were recognized in samples from the interval between 805 and 966 mbsf. All the observed species are characterized by a protoconch and a deutoconch separated by an almost straight wall, strongly resembling *Lepidocyclina canellei*. Following Mitchell et al. (2022) and pending a detailed revision based on modern morphometric criteria of Oligocene and Miocene lepidocyclinids from the American province, these species were not separated. According to Mitchell et al. (2022) and BouDagher-Fadel and Price (2010b), this genus in the American area should extend from the Bartonian to the Burdigalian.

3.4. Geochronology

The U–Pb ages of the reference material (WC-1) yielded intercept ages of 263.23 ± 1.14 Ma, similar to the results obtained by Roberts et al. (2017) of 254 Ma ± 1.6 Ma.

The six samples used to evaluate the dating feasibility were selected based on their abundance within each depth level of the 1-MAS-16-MA core. After collecting information on the U/Pb contents and eliminating outliers from each sample, two treatments were performed with the data obtained.

First, we prepared concords for each corresponding depth interval

**Table 2**

Benthic foraminiferal composition from the Ilha de Santana Formation in the PETROBRAS well 1-MAS-16-MA at section from 510 to 1200 mbsf; D = dominant; Cp = Commonly present; mp = moderately present; rp = rarely present.

Assemblage		mbsf	amphisteginids	miogypsinids	lepidocyclinids	<i>Sphaerogypsina</i>	<i>Victoriella</i>	<i>Heterostegina</i>	planorbulinids	Other nummulitids	<i>Archaias</i>	<i>Sorites</i>	<i>Textularia</i>	<i>Pyrgo</i>	<i>Operculina</i>	<i>Quinqueloculina</i>	Miliolida	<i>Dentalina</i>	SBFhyaline	SBFporcelaneous		
IS - 1	510	D				mp			rp	rp		rp	rp	rp	rp				rp	rp	rp	
	522	D				Cp	rp		rp		rp	rp	rp	rp						rp	rp	mp
	528	D				mp	rp		rp	rp		rp	rp	rp	rp						rp	mp
	534	D				mp	rp		rp	rp				rp								
	540	D				mp	rp		rp													mp
	552	D				rp	rp		rp	rp												rp
	558	D				rp	rp		rp	rp	mp											
	570	D				rp	rp		rp	rp	rp	rp	rp	rp	rp							rp
	580	D				rp	rp		rp	rp	mp											rp
	588	D				rp	rp		rp	mp	rp	rp	rp	rp								
	600	D				rp	rp		rp	rp	rp	rp	rp	rp	rp							rp
	606	D				rp	rp		rp	rp	rp	rp	rp	mp	rp	rp						rp
	624	D				rp	rp		rp	rp			rp	rp	rp	rp	rp					rp
	642	D				rp	rp		rp	rp			rp	rp	rp	rp	rp					rp
IS - 2	660	Cp	rp			rp	rp		rp				rp	rp	rp							rp
	768	D	Cp	rp		rp	rp		rp				rp									rp
	774	D	Cp	mp	rp	rp	rp		rp	rp												rp
	780	Cp	Cp	mp		mp	rp		rp													rp
	786	Cp	D	mp	rp	rp	rp		rp													rp
IS - 3	798	Cp	Cp	mp	rp	rp	rp		rp													rp
	805	Cp	Cp	Cp		rp	rp		rp	rp												rp
	810	Cp	Cp	Cp		rp	rp		rp													rp
	816	Cp	Cp	D	rp	rp	rp		rp	rp												rp
	840	Cp	Cp	Cp	rp	mp	rp		rp													rp
	846	Cp	Cp	Cp	rp	mp	rp		rp													rp
	858	Cp	Cp	Cp	rp	mp	rp		rp													rp
	912	Cp	Cp	Cp		rp	rp		rp													rp
IS - 4	918	Cp	Cp	Cp		rp	Cp	rp	rp	rp												rp
	924	mp	Cp	D		rp	mp	rp	rp													rp
	948	mp	Cp	Cp		mp	Cp		rp		rp											rp
	966	mp	Cp	Cp		rp	Cp		rp													rp
	984	mp	Cp	Cp		mp	Cp		rp													rp
	1008	rp	Cp	Cp		mp	Cp	rp	rp													rp
	1020	rp	Cp	Cp		mp	Cp		rp													rp
	1026	mp	Cp	Cp		rp	Cp		rp													rp
	1032	mp	Cp	Cp		mp	Cp	rp	rp													mp
	1074	mp	mp	Cp		mp	Cp	mp	mp													mp
	1092	mp	mp	Cp		mp	Cp		rp													mp
	1128	mp	rp	Cp		rp	D		rp													rp
	1146	mp	rp	Cp		rp	D		rp													rp
	1164	mp		Cp		rp	D		mp													mp
1200	mp		Cp		Cp	mp		Cp													rp	

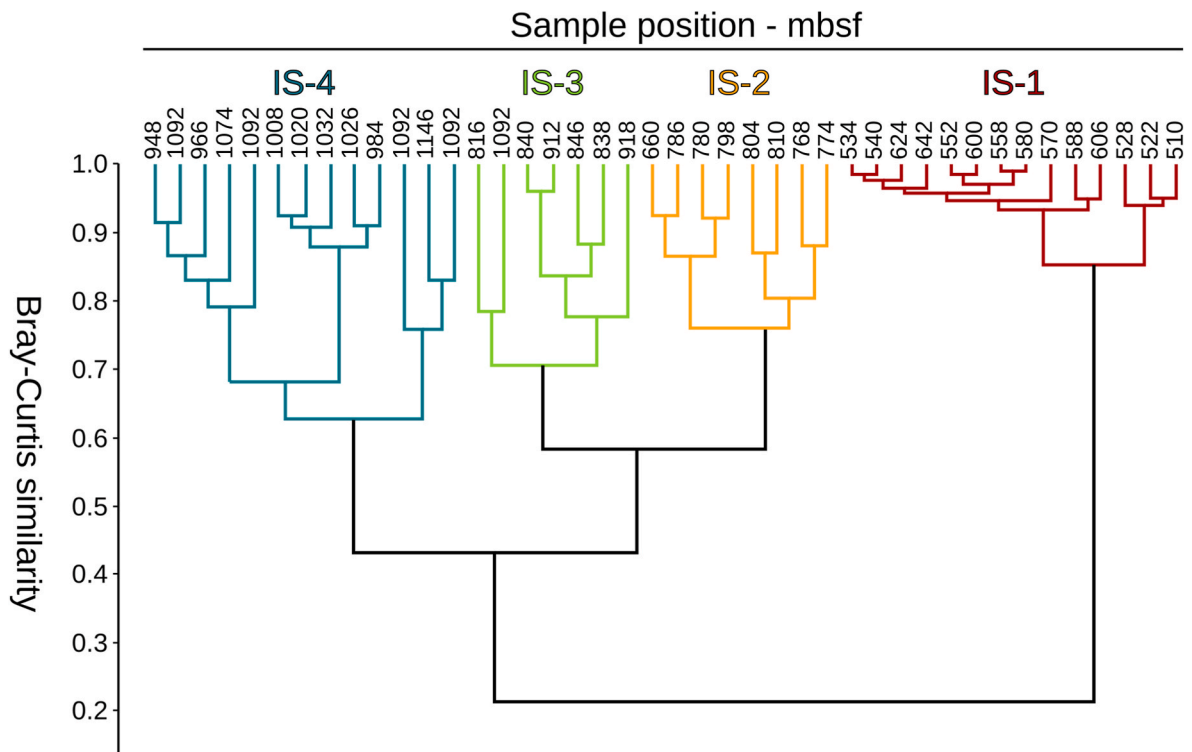


Fig. 4. Multivariate analysis: Bryan Curtis cluster diagram exhibiting the presence of four major groups of foraminiferal assemblages.

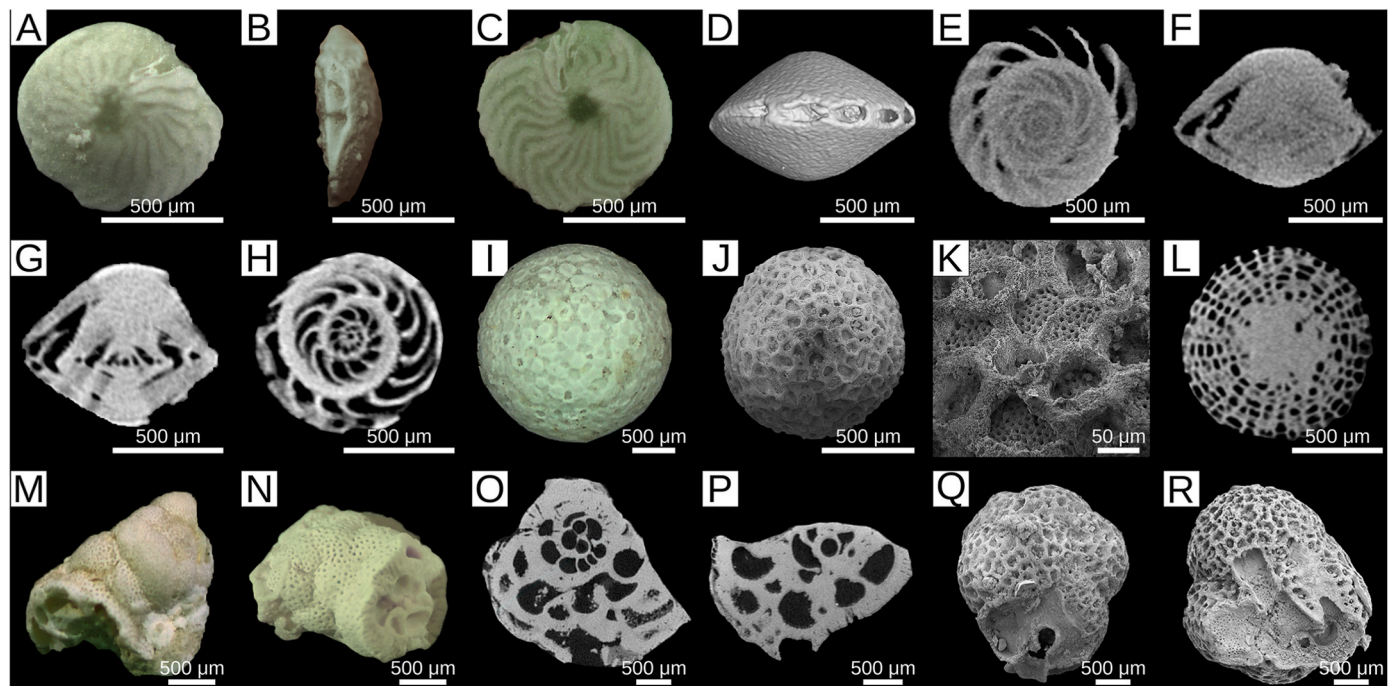


Fig. 5. 1–A, B, C) *Amphistegina* sp., external views, 570 mbsf; D, E, F) *Amphistegina* sp., external view, equatorial and axial sections of the 3D micro-CT model, 570 mbsf; G, H) *Amphistegina* sp., axial and equatorial sections of the 3D micro-CT model, 600 mbsf; I) *Sphaerogypsina* sp., external view, 510 mbsf; J, K) *Sphaerogypsina* sp., SEM external view and detail of the surface, 660 mbsf; L) *Sphaerogypsina* sp., section of the 3D micro-CT model, 774 mbsf; M, N) *Victoriella* sp., external views, 948 mbsf; O, P, Q, R) *Victoriella* sp., equatorial sections of the 3D micro-CT model and external SEM views, 858 mbsf.

(100 m) up to 1000 mbsf. These steps established the limit between the epochs that were clearly visible owing to biostratigraphy. Therefore, although an average of 75 points were made for each of the intervals, and only these points were finally selected, according to the best regression fit (Fig. 11), yielding a relative age for the 600 mbsf interval

of  $17.0 \pm 5.5$  Ma (11.5–22.5 Ma; Serravallian – Aquitanian), for the 700 mbsf interval of  $22.9 \pm 5.7$  (17.2–28.6 Ma; Burdigalian – Rupelian), for the 900 mbsf interval of  $17.9 \pm 3.0$  Ma (14.9–20.9 Ma; Langhian – Aquitanian), and of  $19.6 \pm 7.3$  Ma (12.3–26.9 Ma; Serravallian – Chattian) for the 1000 mbsf interval.



Fig. 6. Photomicrograph of foraminifera in thin sections 1–3) *Amphistegina* sp., 528–510 mbsf; 4) *Heterostegina* sp., 948 mbsf; 5) Planorbulinid, 816 m; 6) Miogypsinid, 846 mbsf; 7) Lepidocyclinid, 1146 mbsf; 8) Lepidocyclinid, 924 mbsf; 9) Lepidocyclinid, 1,200 m; 10) *Heterostegina* sp., 966 mbsf; 11) Heterosteginid, 948 mbsf; 12), *Heterostegina* sp., 948 mbsf; 13) *Victoriella* sp., 624 mbsf; 14) *Victoriella* sp., 1146 mbsf; 15) *Victoriella* sp., 966 mbsf.

## 4. Discussion

### 4.1. Biostratigraphy

Existing data on LBF distribution in the American province (de Mello e Sousa et al., 2003; Robinson, 2004; BouDagher-Fadel and Price, 2010a; BouDagher-Fadel et al., 2010; Mitchell et al., 2022) and world-wide (Cahuzac and Poignant, 1997; BouDagher-Fadel, 2018; Dill et al., 2020) provide useful elements for developing a stratigraphic framework for the analyzed interval of core 1-MAS16-MA (Fig. 3). However, due to the inherent limits of gutter samples, certain intervals could not be confidently assigned at stage level (Fig. 3).

Based on the presence of *Eulepidina* and the lack of miogypsinids and of *Heterostegina* (*Vlerkina*) *antillea*, the base of the studied interval (1200 mbsf), should be placed into the Rupelian. The interval between 1000 and 1100 mbsf can be confidently attributed to the Chattian due to the presence of primitive miogypsinids such as *Miogypsinella* and *Miogypsinoides*. The presence of taxa of *Miogypsina* characterized by a single spire, of *Eulepidina*, and the common occurrence of *Heterostegina* (*Vlerkina*) *antillea*, support this hypothesis (Table 3). The 900–950 mbsf interval can be attributed to Aquitanian, based on the lack of *Miogypsinella* and *Miogypsinoides* and the presence of *Miogypsina tani*, and *H. (Vlerkina) antillea* (Table 3). Between 850 and 660 mbsf a Burdigalian age is suggested by the common presence of taxa of *Miogypsina*

characterized by multiple spires, including *Miogypsina globulina* and *Miogypsina intermedia*, the presence of *Miolepidocyclina*, and the lack of *H. (Vlerkina) antillea* (Table 3). The top of the studied interval of the core should correspond to the Langhian stage, due to the lack of *Victoriella*, miogypsinids, and lepidocyclinids. Although above 660 mbsf there is a sharp decline in the abundance of Early Miocene taxa, the continuous presence of *Victoriella* as well as of some rare (and possibly reworked) miogypsinids does not allow to place the Burdigalian-Langhian boundary with a higher precision. This general stratigraphic framework is in agreement with U–Pb ages, and indicates that the foraminiferal assemblages constrained by similarities analysis (IS-1 to IS-4) have a stratigraphic significance. Higher accuracy could be possibly achieved through more detailed analysis of the biometric features of lepidocyclinids and heterosteginids (Benedetti, 2014; 2021; Benedetti and Schiavinotto, 2022), however, this effort would be greatly hindered by potential reworking issue of cuttings samples.

### 4.2. Paleoenvironmental considerations

During the Cenozoic, the global belt in which larger benthic foraminifera occurred was much broader than it is currently (Adams, 1970). This difference was probably associated with warming global paleoceanographic conditions and increasing sea level. Cenozoic LBF occur abundantly in many platform deposits and can be easily identified at the

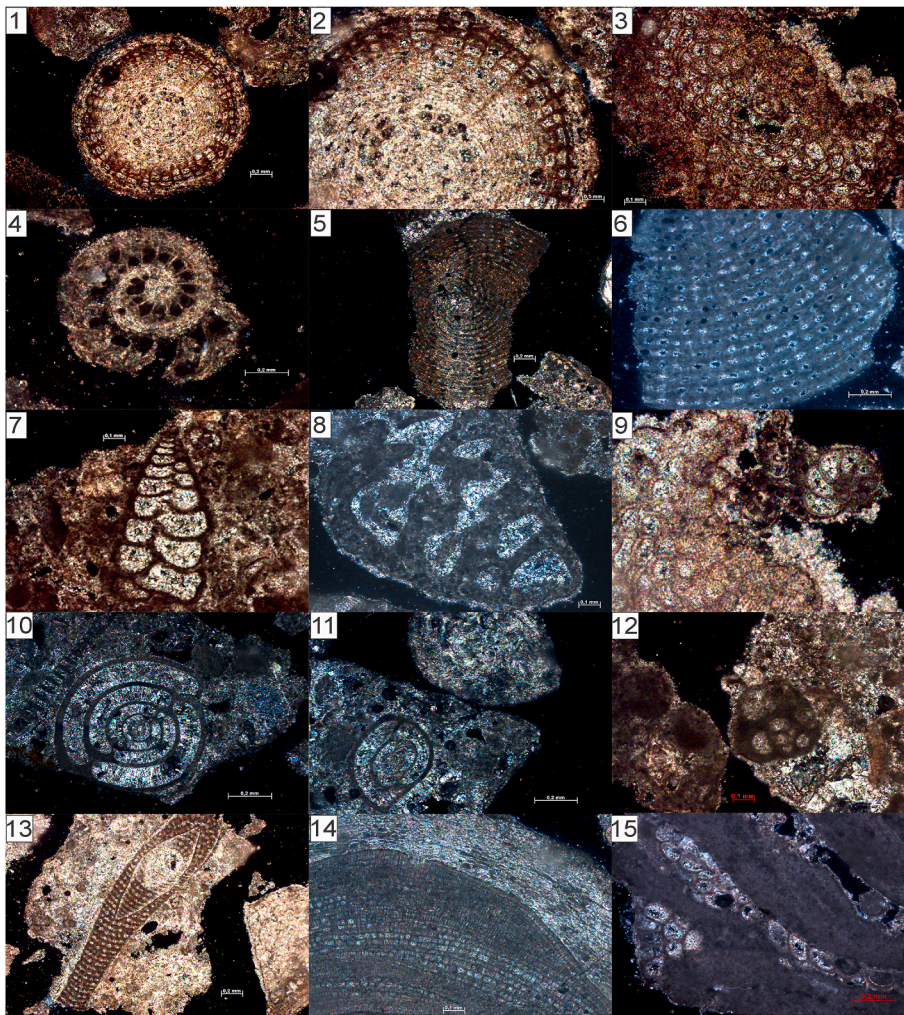


Fig. 7. Photomicrograph of foraminifera and calcareous red algae in thin sections 2. 1–2) *Sphaerogypsina* sp., 510 mbsf; 3) Planorbulinid, 580 mbsf; 4) Nummulitid, 552 mbsf; 5) *Archaias* sp. 600 mbsf; 6) *Sorites* sp., 588 mbsf; 7–8) *Textularia* sp., 510 mbsf; 9) Planorbulinid and a small hyaline benthic foraminifera, 580 mbsf; 10–11) *Pyrgo* sp., 606 mbsf; 12) *Quinqueloculina* sp., 600 mbsf; 13) *Archaias* sp., 588 mbsf; 14) Coralline algae, 606 mbsf; 15) Coralline algae and encrusting benthic foraminifera, 774 mbsf.

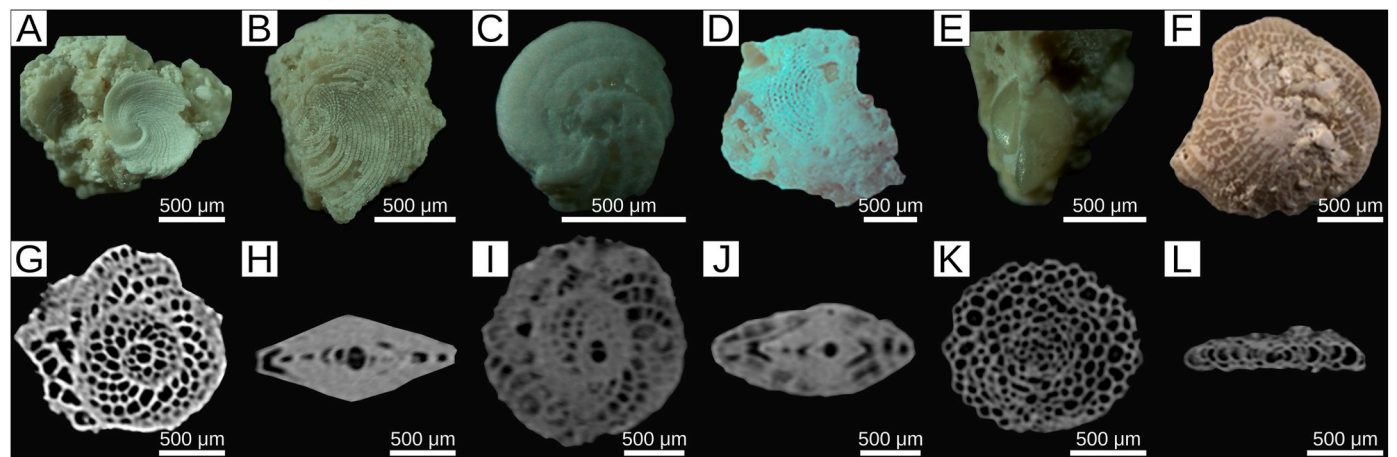
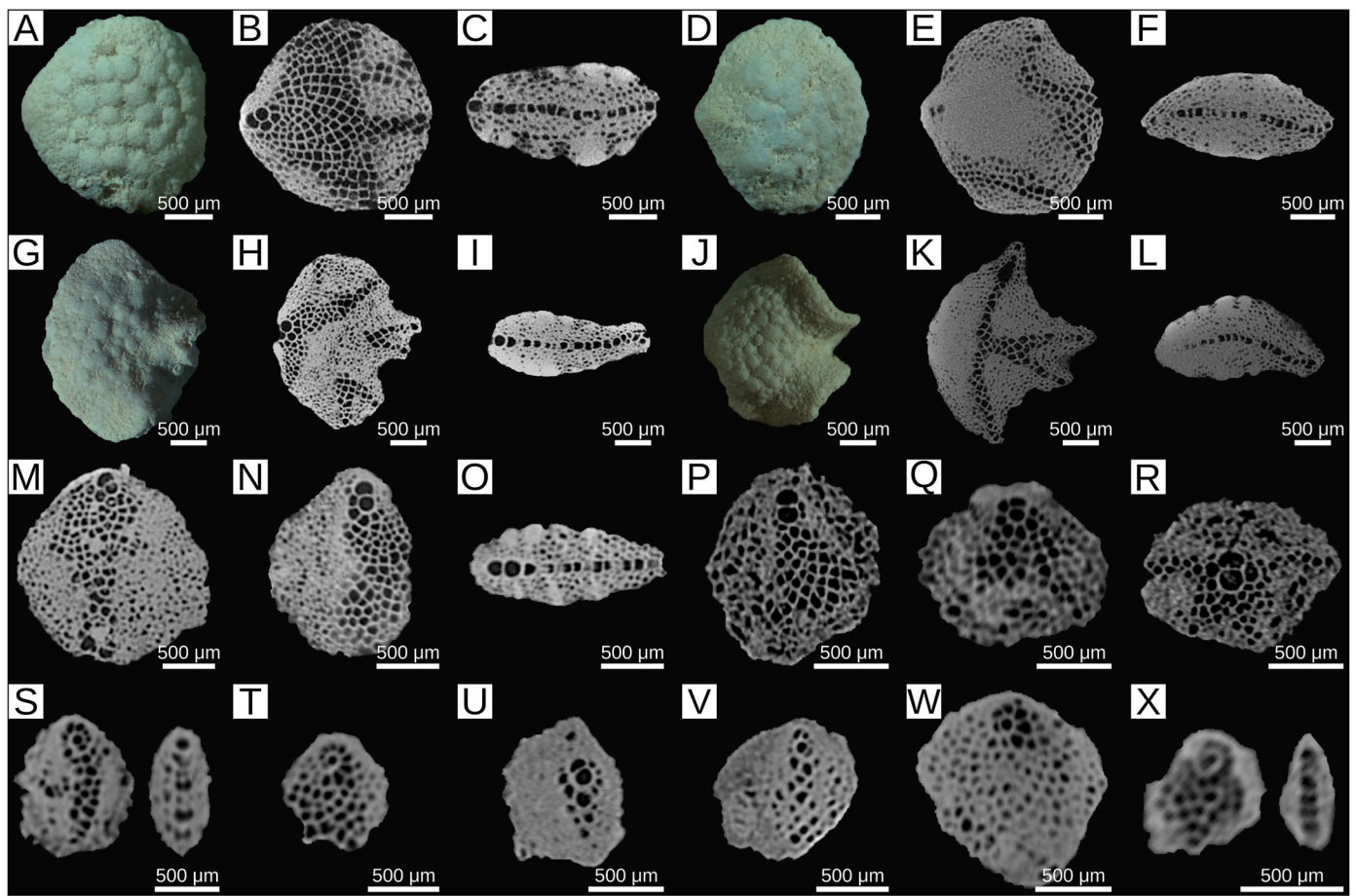


Fig. 8. A) *Archaias* sp., stereomicroscope external view, 570 mbsf; B) *Archaias* sp., stereomicroscope external view, 570 mbsf; C) *Archaias*, stereomicroscope external view, 570 mbsf; D) *Sorites* sp., stereomicroscope external view, 588 mbsf; E) *Pyrgo* sp., stereomicroscope external view, 570 mbsf; F, G, H) *Heterostegina* (*Vlerkina*) *antillea*, external view and equatorial and axial sections of the 3D micro-CT model, 1008 mbsf; I, J) *Heterostegina* (*Vlerkina*) *antillea*, equatorial and axial sections of the 3D micro-CT model, 966 mbsf; K, L) Planorbulinid, equatorial and axial sections of the 3D micro-CT model, 768 mbsf.

genus level (Geel, 2000). Water temperature, nutrients content, light intensity, and hydrodynamic energy controls the global distribution of LBF (Langer and Hottinger, 2000; Beavington-Penney and Racey, 2004; Renema, 2018). Local distribution is controlled by the intensities and

interrelationships of these factors, and abundance is controlled by interspecific competition (Murray, 2006).

Shallow-water carbonate deposits during the Oligocene – Miocene, frequently contain a high diversity of LBF that have been useful for



**Fig. 9.** Photomicrograph and microCT of miogypsinids A, B, C) *Miogypsina globulina*, external view with the stereomicroscope, equatorial and axial sections of the 3D micro-CT model, 660 mbsf; D, E, F) *Miogypsina*, external view with the stereomicroscope, equatorial and axial sections of the 3D micro-CT model, 660 mbsf; G, H, I) *Miogypsina globulina*, external view with the stereomicroscope, equatorial and axial sections of the 3D micro-CT model, 660 mbsf; J, K, L) *Miogypsina*, external view with the stereomicroscope, equatorial and axial sections of the 3D micro-CT model, 660 mbsf; M) *Miogypsina globulina*, 660 mbsf; N, O) *Miogypsina globulina*, equatorial and axial sections of the 3D micro-CT model, 660 mbsf; P) *Miogypsina intermedia*, equatorial section of the 3D micro-CT model, 805 bsf; Q) *Miogypsina globulina* equatorial section of the 3D micro-CT model, 918 bsf; R) *Miolepidocyclina*, equatorial section of the 3D micro-CT model, 805 mbsf; S) *Miogypsina gunteri*, equatorial and axial sections of the 3D micro-CT model, 1032 mbsf; T) *Miogypsina gunteri*, equatorial section of the 3D micro-CT model, 1026 mbsf; U) *Miogypsina gunteri*, equatorial section of the 3D micro-CT model, 1032 mbsf; V) *Miogypsina gunteri*, equatorial section of the 3D micro-CT model, 1032 mbsf; W) *Miogypsina gunteri*, equatorial section of the 3D micro-CT model, 1032 mbsf; X) *Miogypsinella*, equatorial and axial sections of the 3D micro-CT model, 1008 mbsf.

biostratigraphy, paleoenvironmental interpretations, and paleobiogeography of shallow-marine deposits of the Western Tethys, the Middle East, the Indo-Pacific region, and of Central America (Adams, 1970; Cahuzac and Poignant, 1997; Van Vessem, 1978; Butterlin, 1984; de Mello e Sousa et al., 2003; Robinson, 2004; Özcan et al., 2009; BouDagher-Fadel et al., 2010; BouDagher-Fadel, 2018; Briguglio, 2018; Dill et al., 2020). Similarly, to other coeval South American shallow water carbonates (Aguilera et al., 2020b), the Ilha de Santana Formation is dominated by RCA and benthic foraminifera, associated with minor amounts of heterozoan shallow-marine biota (mollusks, bryozoans, and echinoderms). The remarkable abundance and diversity of LBF suggest an overall warm climate during the whole investigated interval (Beavington-Penney and Racey, 2004). Based on the characteristic of the skeletal and foraminiferal assemblage it is also possible to provide a paleoenvironmental interpretation of the various biofacies.

BF-7 is characterized by the dominance of RCA and the common presence of lepidocyclinids, victoriellids, and nummulitids (*Operculina*, and possibly *Nummulites*). The abundance RCA and hyaline LBF and the lack of planktic foraminifera, suggest an environment in the middle to lower part of the photic zone (mesophotic to oligophotic conditions, *sensu* Pomar, 2001; Hallock and Glenn, 1986). A similar interpretation can be proposed for BF-6 that, similarly to BF-7, is dominated by hyaline

LBF and RCA. RCA and hyaline LBF also dominates in BF-5, however, the abundance of encrusting benthic foraminifera (mainly *Victoriella*) and of miogypsinids might suggest slightly shallower conditions (around 10 m less than BF-6) and the nearby presence of a bioconstruction. Miogypsinids are known to occur in shallower conditions compared to lepidocyclinids and heterosteginids and are often found either close or directly associated with reefs (Geel, 2000; BouDagher-Fadel, 2018; Coletti et al., 2021). Encrusting benthic foraminifera are a common component of Cenozoic shallow-water bioconstructions and victoriellids are known to occur in shallow to middle depth settings often associated with reefs (Campbell et al., 1988; Perrin, 1992). A decrease in relative water depth is also supported by the abundance of marly layers, which are absent in the interval characterized by BF-5 but occur in the interval characterized by BF-6. Similarly, to the other biofacies characterized by the IS-4 foraminiferal assemblage, BF-4 can be related to a middle platform setting. However, it displays notable differences in comparison to the underlying BF-5, namely a lower amount of miogypsinids and of encrusting benthic foraminifera and a higher amount of lepidocyclinids. This suggests a slight increase in water depth with respect to BF-5. Drilling operation reports also indicate the presence of a dolomite layer separating the two biofacies, further highlighting that a relevant event occurred between the deposition of the intervals characterized by

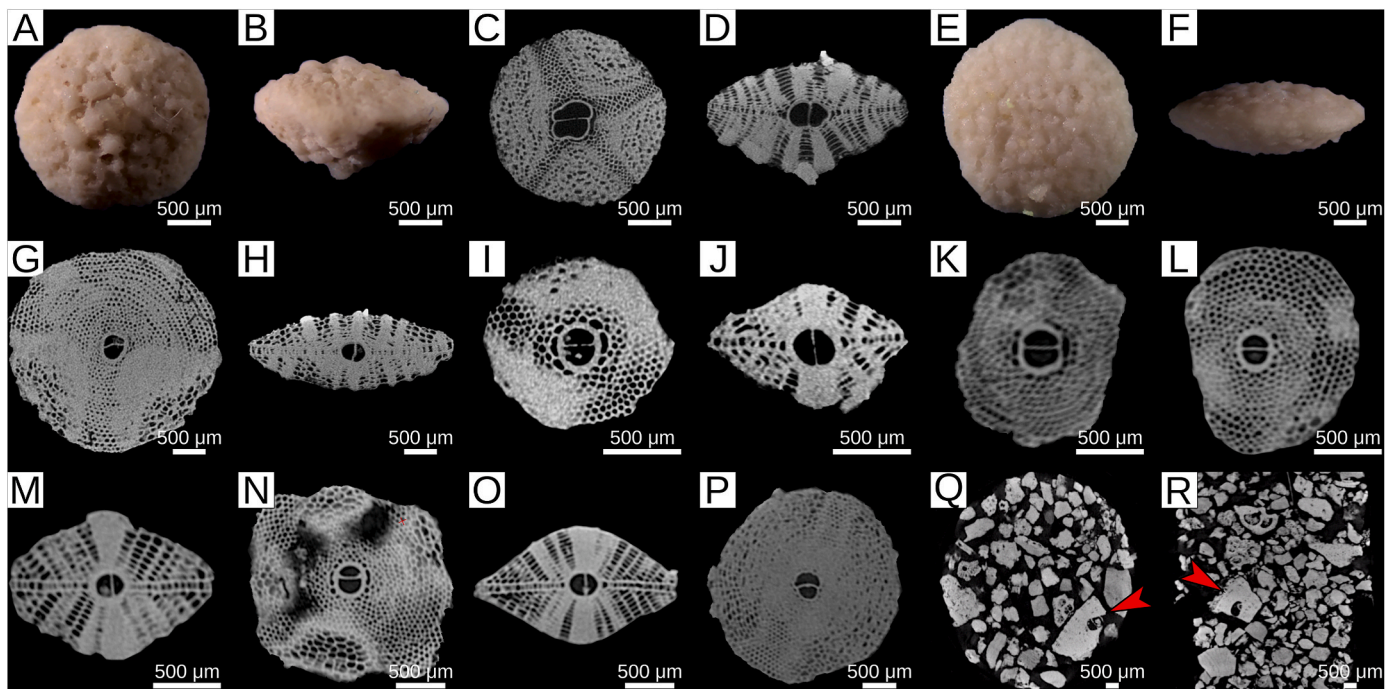


**Fig. 10.** Photomicrograph and microCT of lepidocyclinids. A, B, C, D) *Lepidocyclus* sp., external views, equatorial and axial sections of the 3D micro-CT model, 816 mbsf; E, F, G, H) *Lepidocyclus* sp., external views, equatorial and axial sections of the 3D micro-CT model, 816 mbsf; I, J) *Lepidocyclus* sp., equatorial and axial sections of the 3D micro-CT model, 816 mbsf; K) *Lepidocyclus* sp., equatorial sections of the 3D micro-CT model, 918 mbsf; L, M) *Lepidocyclus* sp., equatorial and axial sections of the 3D micro-CT model, 924 mbsf; N, O) *Lepidocyclus* sp., equatorial and axial sections of the 3D micro-CT model, 924 mbsf; P) *Lepidocyclus* sp., equatorial sections of the 3D micro-CT model, 948 mbsf; Q, R) Fragment of *Eulepidina* sp. observed in the Eppendorf micro-ct scan of sample, red arrowhead = *Eulepidina* fragment, 1200 mbsf.

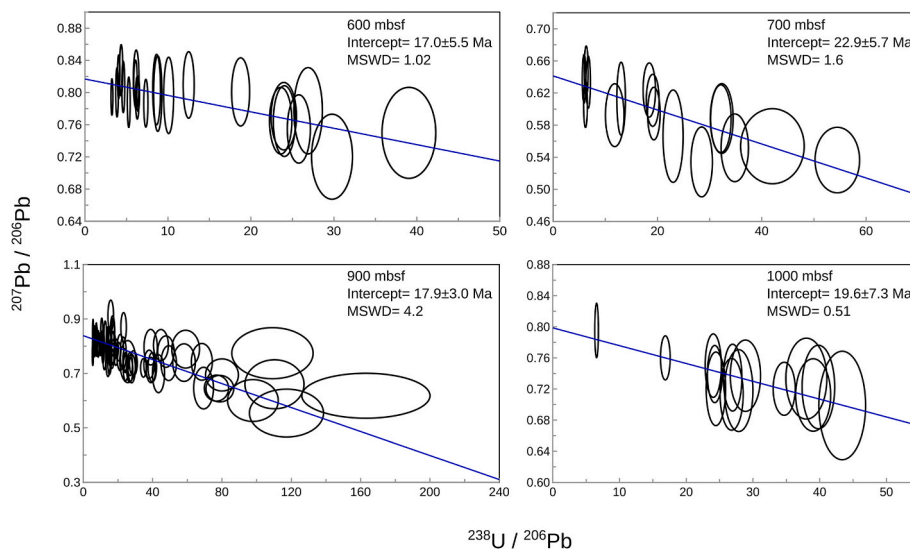


**Fig. 11.** U-Pb Tera-Wasserburg plots for the analysis of carbonate samples (LBF and coralline algae).

the two facies (Fig. 2). These elements are consistent with the stratigraphic framework based on LBF that suggests that the Oligocene – Miocene boundary is located between BF-5 and BF-4. Global paleoclimatic records suggest that a rapid and major glacial expansion occurred in Antarctica across the Oligocene – Miocene transition (c. 23 Ma; ~50 m sea level equivalent in 200–300 kyr) (Greenop et al., 2019). Such an event could explain the pattern of decreasing and then increasing water depth across the Oligocene – Miocene boundary as recorded by the BF-5 – BF-4 interval of core 1-MAS-16-MA.

Biofacies BF-3 is characterized by a peak in the relative abundance of both lepidocyclinids and bryozoans suggesting a further small increase

in water depth with respect to the underlying BF-4. A remarkable increase in the abundance of miogypsinids can be instead observed in the interval characterized by BF-2, with miogypsinids clearly dominating the foraminiferal assemblage (IS-2) and the skeletal assemblage. In comparison with the underlying BF-3 the contribution of bryozoans also decreases while the contribution from corals and *Halimeda* increase. These differences are most likely related to a decrease in water depth and a consequent increase in light availability at the sea-floor. A further, albeit slight, decrease in water depth is testified by BF-1 which is characterized by a foraminiferal assemblage with moderately common porcelanaceous foraminifera, including taxa, like *Sorites* and *Archaias*,

Table 3

Biometric parameters of measured individuals of age diagnostic species of LBF; avg= average, max= maximum, min= minimum.

Taxon	PW (μm)	PH (μm)	DW (μm)	DH (μm)	β (°)	α (°)	γ (°)	N	SW	IPP	Ai (%)	NACII	V
<i>Lepidocyclus</i> sp. (avg)	265	180	290	135					275	760	37	2.5	
(max)	370	300	400	195					395	1135	42	4	
(min)	165	95	180	75					160	470	32	1	
(number of measured specimens)	14	14	14	14					14	14	14		
<i>Miogypsina globulina</i> (avg)	135	115	145	70	225	45	20	5.5					39
(max)	160	145	185	95	238	50	65	6					44
(min)	105	85	105	52	210	35	0	5					30
(number of measured specimens)	6	6	5	5	6	6	6	6					6
<i>Miogypsina intermedia</i> (avg)	130	105	160	95	220	65		4.5					60
(max)	165	135	200	105	236	80		5					70
(min)	100	79	135	76	185	50		4					55
(number of measured specimens)	3	3	3	3	3	3		3					
<i>Miogypsina gunteri</i> (avg)	75	70	80	45	295		-75	9					
(max)	115	100	115	55	360		90	11					
(min)	55	55	60	40	200		-140	8					
(number of measured specimens)	7	7	5	5	3		6	6					
<i>Miogypsina tani</i> (avg)	135	110	105	50	155		-75	6					
(number of measured specimens)	2	2	2	2	2	2	2	2					
<i>Heterostegina (Vlerkina) antillea</i> (avg)	145	125											
(max)	220	180											
(min)	80	80											
(number of measured specimens)	8	8											

which are commonly associated with seagrass meadows (Murray, 2006) and thus to euphotic conditions (*sensu* Pomar, 2001).

#### 4.3. LBF distribution during the Oligocene – early Miocene interval in the South American province

Adams (1970, 1983) established three Tertiary Faunal Provinces for larger benthic foraminiferal assemblages: 1) Central America, 2) Tethys, and 3) Indo-West Pacific. The Southern American province, on the other hand, has only been studied sparsely throughout the years due to the lack of outcropping sedimentary successions deposited during the Cenozoic. For this reason, the succession of core 1-MAS-16-MA represents a unique opportunity for studying LBF distribution in the area. Although drill cuttings do not allow to properly assess textures and have contamination and reworking issues (Sanei et al., 2020), the detailed examination of both skeletal and foraminiferal assemblages, performed with micro-CT scan, stereomicroscope, SEM and thin sections analysis, allowed the recognition of relevant biostratigraphical and paleoenvironmental trends within the studied interval of the Ilha de Santana Formation of the Pará-Maranhão Basin.

From the point of view of paleoenvironmental reconstruction, the base of the Oligocene interval (1200 - 950 mbsf) records a middle platform environment that, in the upper part of the interval, close to the Oligocene – Miocene boundary, becomes progressively shallower. The lower part (950–850 mbsf) of the Miocene interval testifies instead of a progressive sea level rise, culminating with the deposition of BF-3. The upper part of the Miocene interval (850–510) suggests a progressive shallowing, with the uppermost part of the studied interval of the core displaying skeletal and foraminiferal assemblages suggestive of a proximal middle platform environment close to the lower limit of seagrass meadows distribution. With regards to LBF stratigraphy, it is possible to recognize different fossiliferous assemblages for each stage: 1) Rupelian assemblages are characterized by nummulitids and lepidocyclinids (mainly *Eulepidina*); 2) Chattian assemblages by the abundance of *Heterostegina (Vlerkina) antillea*, lepidocyclinids, and primitive miogypsinids (*Miogypsinella*, *Miogypsinoides* and single-spire species of *Miogypsina*); 3) Aquitanian assemblage by the abundance of *Heterostegina (Vlerkina) antillea*, lepidocyclinids, and miogypsinids, except primitive taxa such as *Miogypsinoides* and *Miogypsinella*; 4) Burdigalian assemblage by the disappearance of *H. (Vlerkina) antillea*, and the dominance of highly evolved miogypsinids such as *Mioplepidocyclina* and multi-spiral *Miogypsina*; 5) Middle Miocene assemblages by the absence

of abundant lepidocyclinids and miogypsinids.

Similar paleoenvironmental and biostratigraphic patterns can be observed in the successions of Southern and Central America. The analysis of BouDagher-Fadel et al. (2010) of the Campos Basin (South-eastern Brazilian Margin) highlighted the presence of several, age-diagnostic, benthic foraminiferal biozones within the Oligocene – Miocene interval: Rupelian assemblages dominated by lepidocyclinids; late Rupelian to Chattian assemblages dominated by lepidocyclinids, miogypsinids (mainly primitive taxa), heterosteginids, and amphisteginids; Aquitanian assemblages characterized by abundant miogypsinids (mainly evolved taxa), lepidocyclinids, and amphisteginids; Burdigalian assemblages characterized the abundant evolved miogypsinids. Similarly, to core 1-MAS-16-MA, the successions of the Campos Basin records a deepening of the depositional environment during the Burdigalian. However, whereas in 1-MAS-16-MA this trend quickly reverts, a progressive increase in the relative sea-level is recorded throughout the whole Lower and Middle Miocene interval of the Campos Basin.

Several similarities can be observed also with the White Limestone Group of Jamaica studied by Robinson (2004). Based on LBF distribution and supported by Strontium isotopes stratigraphy several age-diagnostic foraminiferal assemblages are recognized: Rupelian assemblages largely dominated by lepidocyclinids (including *Eulepidina*); Chattian assemblages dominated by lepidocyclinids (including *Eulepidina*), *Heterostegina (Vlerkina) antillea* and, in the upper Chattian, also dominated by primitive miogypsinids; Aquitanian assemblages dominated by evolved miogypsinids, lepidocyclinids, and *H. (Vlerkina) antillea*; Burdigalian assemblages dominated by evolved miogypsinids; Middle Miocene assemblages lacking both miogypsinids and lepidocyclinids. Differently from core 1-MAS-16-MA, the succession of the White Limestone Group does not display a wide variety of miogypsinids taxa.

Parallels also exist with the succession of the Foz do Amazonas Basin examined by de Mello e Sousa et al. (2003): Rupelian assemblages are dominated by lepidocyclinids and lack both miogypsinids and *Heterostegina (Vlerkina) antillea*; late Oligocene to Aquitanian assemblages are dominated by lepidocyclinids and *H. (Vlerkina) antillea*; Aquitanian to Burdigalian assemblages are dominated by miogypsinids; Burdigalian to early Langhian assemblages are characterized by the lack of lepidocyclinids, *H. (Vlerkina) antillea* and the scarcity of miogypsinids (only very rare specimens of *Miogypsina globulina*). Similarly, to 1-MAS-16-MA, a relative rise in sea level is recorded close to the Aquitanian – Burdigalian boundary, followed by a decrease in sea level

during the Burdigalian – Langhian interval.

Foraminiferal assemblages comparable to IS-1 of core 1\_MAS-16-MA occur also in the upper Pirabas Formation. The latter represents the youngest, chiefly bioclastic, interval of the Cenozoic succession of the Brazilian passive margin and is the onshore equivalent of the offshore units of the Pará-Maranhão Basin (Nogueira et al., 2021; Aguilera et al., 2022). The outcrops of the Pirabas Formation commonly display a foraminiferal assemblage dominated by amphisteginids and soritids and lacking both miogypsinids and lepidocyclinids (Aguilera et al., 2022). Based on palynological studies performed on these outcrops, the upper Pirabas Formation should have formed between the late Burdigalian and the Late Miocene (Gomes et al., 2023).

This regional comparison sparks two relevant considerations. 1) Both the Pará-Maranhão and Foz do Amazonas basins record the same pattern of relative sea-level oscillations during the Miocene (increase in relative sea-level during the Aquitanian – early Burdigalian followed by a decrease during the late Burdigalian – Langhian), which differs from that of the Campos Basin. This indicates an overall common behavior of the two close-by basins of the northern equatorial margin during the Miocene, a behavior that is different from the one of the southern portion of the margin. 2) The Central and Southern American bioprovince displays a similar LBF stratigraphy in the Oligocene – Miocene interval. This zonation was initially identified by Butterlin (1981, 1987) and Abreu et al. (1986) and later refined by Robinson (2004), but poorly tested along the Atlantic South American coast. The age diagnostic relevance of these foraminiferal assemblages is supported by absolute dating, namely by Sr isotope stratigraphy in Jamaica (Robinson, 2004) and, albeit with a much lower accuracy, by the U/Pb dating performed in this study. Although the precise timing of certain events (e.g., first and last occurrence of several miogypsinids taxa or the last occurrence of *Heterostegina (Vlerkina) antillea*), is still uncertain, the main elements of the zonation (e.g., the dominance of evolute miogypsinids during the Burdigalian) can be observed in the whole Central and South American bioprovince. This implies a strong interconnection between the various areas of the province, fostering the rapid spreading of the various taxa of LBF.

Similarities and difference can be also observed with the scheme of biozones used in the Mediterranean (Cahuzac and Poignant, 1997); Middle East (Dill et al., 2020) and East Asia (Adams, 1970). However, the lack of standardized data on the biometry of the various stratigraphically significant species of LBF and on their abundance in the different assemblages of the different regions prevents an accurate and detailed comparative analysis from being performed.

It is also worth noting that although the Oligocene – Miocene transition corresponds to a major environmental event, within the succession of core 1-MAS-16-MA, does not correspond to a major faunal turnover. The transition is actually recorded into the core, most likely by the dolomite layer, but the assemblages above and below are similarly characterized by the dominance of RCA and of various groups of LBF and no major variations in the overall foraminiferal assemblage are recognized using similarity analysis. Similarity to 1-MAS-16-Ma, also in the succession of Foz do Amazonas Basin the Oligocene – Miocene boundary is not clearly placed (de Mello and Sousa et al., 2003: Fig. 4). In the Campos Basin the main faunal turnover does not take place at the Oligocene – Miocene boundary but at the Burdigalian – Langhian boundary (BouDagher-Fadel et al., 2010). Similarly, to the Campos Basin, also in the examined interval of core 1-MAS-16-MA the main faunal turnover occur at the Burdigalian – Langhian boundary, with the disappearance of abundant miogypsinids and lepidocyclinids from the assemblage. This large scale event is recorded, at the same time, into the Mediterranean (Cahuzac and Poignant, 1997). In the Indo-Pacific both groups survived for longer (Adams, 1970). The reason of the extinction of miogypsinids and lepidocyclinids and of the associated decrease in LBF diversity (BouDagher-Fadel, 2018) is not clear yet, but could be connected with the progressive segmentation of the Tethys, since the closure of the connection between the Mediterranean and the

Indo-Pacific was essentially completed by the end of the Early Miocene (Bialik et al., 2019). LBF became one of the most important (if not the most important) group of benthic carbonate producers following the very warm interval comprised between the end of the Palaeocene and the early Eocene (Coletti et al., 2022). However, their relevancy significantly outlasted the greenhouse period of the early Paleogene and extended well into the Neogene, suggesting that their adaptability allowed them to take advantage of the decline of their competitors and keep this lead for a long time (Coletti et al., 2022). The relatively mild effect of the Oligocene – Miocene transition recorded in the succession of core 1-MAS-16-MA and in Central and Southern American provinces further demonstrates LBF's capacity to endure and prosper in the face of the majority of environmental changes.

## 5. Conclusions

The analysis of the 500–1200 mbsf interval of the succession of core 1-MAS-16-MA of the Ilha de Santana Formation, using a combination of thin sections, stereomicroscope, SEM, and micro-CT scan observations allowed for the identification of four foraminiferal assemblages and seven biofacies. Assemblage IS-4 is dominated by nummulitids (mainly heterosteginids), associated with common lepidocyclinids and *Victoriella*, and is of Oligocene age. Assemblages IS-3, IS-2 and IS-1, which are dominated by miogypsinids, amphisteginids, and lepidocyclinids, are of Miocene age. Further details on the stratigraphy were provided by the analysis of the distribution of certain age diagnostic taxa and by U/Pb dating of biogenic carbonate. Based on the characteristics of the skeletal assemblage it was possible to further separate the core in seven biofacies. Although all of them are dominated by red calcareous algae and hyaline large benthic foraminifera suggesting a deposition in a middle depth platform environment, changes in foraminiferal abundance allowed for the recognition of paleoenvironmental variations. The base of the Oligocene interval (BF-6 and BF-7) records an average middle platform environment while upwards the increase in miogypsinids and victoriellids indicates slightly shallower conditions (BF-5). The Aquitanian (BF-4) and lower Burdigalian (BF-3) testify for a progressive deepening of the depositional environment suggested by the increase in lepidocyclinids and bryozoans abundance. The upper part of the Burdigalian interval (BF-2) and the Langhian interval (BF-1) indicate a reverse of the previous trend of relative sea-level rise and a progressive shallowing from the deeper portion of the middle platform towards the boundary between the middle platform and the inner platform. The same sequence of sea-level variations can be also observed in the nearby Foz do Amazonas Basin, indicating a common behavior of the two basins. The combination of both skeletal and foraminiferal assemblages allowed also to recognize the typical fossil assemblage of each stage, namely: Rupelian assemblages are characterized by nummulitids and lepidocyclinids (mainly *Eulepidina*) abundance; Chattian assemblages are characterized by the abundance of *Heterostegina (Vlerkina) antillea*, lepidocyclinids, and primitive miogypsinids (*Miogypsinella*, *Miogypsinoides*, and single-spire species of *Miogypsina*); Aquitanian assemblages are characterized by the abundance of *Heterostegina (Vlerkina) antillea*, lepidocyclinids, and miogypsinids (excluding primitive taxa such as *Miogypsinoides* and *Miogypsinella*); Burdigalian assemblages are characterized by the lack of *H. (Vlerkina) antillea* and the abundance of highly evolved miogypsinids such as multi-spiral *Miogypsina*; Middle Miocene assemblages are characterized by the absence of abundant lepidocyclinids and miogypsinids. This pattern can be observed also in other areas of Central and Southern American providing an instrument for basic correlation of bioclastic sedimentary successions useful for both hydrocarbon exploration and paleontological researches. The Oligocene – Miocene transition recorded into the core between biofacies BF-4 and BF-5, is represented by only moderate changes in the fossil assemblage, and in particular in the large benthic foraminiferal assemblage, indicating the overall resilience of large benthic foraminifera to large-scale environmental perturbations.

## Author contributions

O.A., G.C. and D.A.S., designed the research. D.A.S., O.A., O.M.O.A., R.T.L., G.C., and M.G., performed the laboratory analyses and the research. D.A.S., O.A., O.M.O.A., R.T.L., G.C., M.G., B.T.G., A.P.L., and V.T.K., contributed data. D.A.S., O.A., O.M.O.A., R.T.L., G.C., M.G., V.T.K., and M.V.A.A., analyzed data. D.A.S., O.A. and G.C., drafted figures. D.A.S., O.A. and G.C., wrote the paper. All authors performed the manuscript review.

## Funding

This study was supported by the Brazilian Council of Science and Technological Development (CNPq) (grant 404,937/2018–7, grant INCT-ANAIS 406303/2022–3 to RL) and productivity fellowships (305,269/2017–8, 304,693/2021–9 to OA; 314,225/2021 to RTL), and Fundação Carlos Chagas Filho de Amparo à Pesquisa do Estado do Rio de Janeiro (FAPERJ) (grant E–26/201.035/2021 to OA), and the Coordination for the Improvement of Higher Education Personnel (CAPES), finance code 001 (Brazil) to D.A.S. and B.T.G.

## Competing financial interests

The authors declare no competing interests.

## Declaration of competing interest

The authors declare no competing interest.

## Data availability

No data was used for the research described in the article.

## Acknowledgments

The authors would like to thank the National Agency of Petroleum (ANP) and PETROBRAS, Brazil; the Federal University of Pará, Post-graduation Program in Geology and Geochemistry; the Federal Fluminense University, Department of Marine Biology and the Postgraduation Program of Environmental Geochemistry; the Federal University of Rio de Janeiro, Nuclear Engineering Program; The Rio de Janeiro State University; The Paraense Emilio Goeldi Museum; We thank C. Lamarão, J. Lobos, H. Costi, and J. Dos Santos Silva for valuable assistance. The authors are also grateful to two anonymous reviewers whose comment significantly improved the paper and to the editors of the journal for their help and their support. Special thanks also to C. Jaramillo and C. Ng for a review of an early version of the manuscript.

## References

- Abreu, W.S., Regali, M.P., Shimabukuro, S., 1986. O Terciário da plataforma continental do Maranhão e Pará, Brasil: biostratigrafia e evolução paleoambiental. *Anais do 34 Congresso Brasileiro de Geologia*. Goiânia. 1, 145–156.
- Adams, C.G., 1970. A reconsideration of the East Indian letter classification of the Tertiary. *Bull. Br. Mus. (Nat. Hist.) Geol.* 19 (3), 85–137.
- Adams, C.G., 1983. In: Sims, R.W., Price, J.H., Whalley, P.E.S. (Eds.), *Evolution, Time and Space: The Emergence of the Biosphere*, 23. Systematics Association, Special, pp. 255–289.
- Aguilera, O., Oliveira de Araújo, O.M., Hendy, A., Nogueira, A.A.E., Nogueira, A.C.R., Maurity, C.W., Kutterd, V.T., Martins, M.V.A., Coletti, G., Borba, B., Silva-Caminha, S.A.F., Jaramillo, C., Bencomo, K., Lopes, R.T., 2020a. Palaeontological framework from Pirabas Formation (North Brazil) used as potential model for equatorial carbonate platform. *Journal of Marine Micropaleontology* 154, 1–23. <https://doi.org/10.1016/j.jarmicro.2019.101813>.
- Aguilera, O., Bencomo, K., de Araújo, O.M.O., Dias, B.B., Coletti, G., Lima, D., Silane, A. F., Polk, M., Alves-Martin, M.V., Jaramillo, C., Kutter, V.T., Lopes, R.T., 2020b. Miocene heterozoan carbonate systems from the western Atlantic equatorial margin in South America: the Pirabas Formation. *Journal of Sedimentary Geology* 407, 105739.
- Aguilera, O., Martins, M.V.M., Linhares, A.P., Kütter, V.T., Coletti, G., 2022. Palaeoenvironment of the Miocene Pirabas Formation mixed carbonate–siliciclastic deposits, Northern Brazil: insights from skeletal assemblages. *Mar. Petrol. Geol.* 145, 105588 <https://doi.org/10.1016/j.marpetgeo.2022.105585>.
- Banner, F.T., Hodgkinson, R.L., 1991. A revision of the foraminiferal subfamily Heterostegininae. *Rev. Espanola Micropaleontol.* 23 (2), 101–140.
- Beavington-Penney, S.J., Racey, A., 2004. Ecology of extant nummulitids and other larger benthic foraminifera: applications in palaeoenvironmental analysis. *Earth Sci. Rev.* 67 (3–4), 219–265.
- Benedetti, A., 2014. Spiral growth in *Nephrolepidina*: evidence of “golden selection”. *Paleobiology* 40, 151–161.
- Benedetti, A., 2021. *Spira mirabilis* in *Heterostegina*: evolutionary and ecological perspectives. *Hist. Biol.* 33 (10), 2171–2181.
- Benedetti, A., Schiavinotto, F., 2022. Evolutionary trends in the Mediterranean *Nephrolepidina*: new chronosubspecies and biostratigraphic constraints. *Historical Biology* 35 (4), 518–536. <https://doi.org/10.1080/08912963.2022.2054711>.
- Bialik, O.M., Frank, M., Betzler, C., Zammit, R., Waldmann, N.D., 2019. Two-step closure of the miocene Indian ocean gateway to the mediterranean. *Sci. Rep.* 9 (1), 8842.
- BouDagher-Fadel, M.K., 2018. *Evolution and Geological Significance of Larger Benthic Foraminifera*, second ed. UCL Press, London. <https://doi.org/10.14324/111.9781911576938>.
- BouDagher-Fadel, M.K., Price, G.D., 2010a. American Miogypsinidae: an analysis of their phylogeny and biostratigraphy. *Micropaleontology* 567–586.
- BouDagher-Fadel, M.K., Price, G.D., 2010b. Evolution and paleogeographic distribution of the lepidocylinids. *J. Foraminif. Res.* 40 (1), 79–108.
- BouDagher-Fadel, M.K., Price, G.D., Koutsoukos, E.A.M., 2010. Foraminiferal biostratigraphy and paleoenvironments of the Oligocene-Miocene carbonate succession in Campos Basin, southeastern Brazil. *Stratigraphy* 7 (4), 283–299.
- Brandão, J.A.S.L., Feijó, F.J., 1994. Bacia do Foz do Amazonas. *Bol. Geociencias Petrobras* 8 (1), 91–100.
- Briguglio, A., 2018. The Miocene (Burdigalian) lepidocylinids and miogypsinids of Channa kodi, Padappakkara, Kerala, southern India. *Palaeontogr. Abt. A Palaeozool.-Stratigr.* 312, 1–15.
- Butterlin, J., 1981. Claves para la determinación de macroforaminíferos de México y del Caribe, del Cretácico Superior al Mioceno Medio. Instituto Mexicano del petróleo, p. 1.
- Butterlin, J., 1984. Notes on some larger foraminifera from the Tertiary of the French Lesser Antilles and on the phylogeny of American species of the genus *Lepidocyclus*. *Bulletin des centres de recherches exploration-production Elf-Aquitaine - Memoir.* 6, 105–115.
- Butterlin, J., 1987. Origine et évolution des Lépidocyclines de la région des Caraïbes. Comparaisons et relations avec les Lépidocyclines des autres régions du Monde. *Rev. Micropaleontol.* 29 (4), 203–219.
- Cahuzac, B., Poignant, A., 1997. Essai de biozonation de l'Oligo-Miocène dans les bassins européens à l'aide des grands foraminifères néritiques. *Bull. Soc. Geol. Fr.* 168 (2), 155–169.
- Campbell, H.J., Andrews, P.B., Beu, A.G., Edwards, A.R., Hornibrook, N.D., Laird, M.G., Maxwell, P.A., Watters, W.A., 1988. Cretaceous-cenozoic lithostratigraphy of the chatham islands. *J. Roy. Soc. N. Z.* 18 (3), 285–308.
- Cardoso, L.M.C., Santos, T.J.S., Romero, L.F., Geraldes, M.C., Ganade, C.E., 2023. U-Pb ages via LA-ICP-MS of carbonate from brittle structures of Jandaíra Formation, Potiguar Basin, NE-Brazil. *Journal of South American Earth Sciences* 125, e104316. <https://doi.org/10.1016/j.jsames.2023.104316>.
- Carey, J.S., Moslow, T.F., Barrie, J.V., 1995. Origin and distribution of Holocene temperate carbonates, Hecate Strait, western Canada continental shelf. *J. Sediment. Res. Section A Sedimentary Petrology and Processes* 65 (1), 185–194.
- Clarke, K.R., Gorley, R.N., 2006. *PRIMER V6: User Manual/Tutorial*. PRIMER-E, Plymouth, p. 192.
- Coletti, G., Basso, D., Frixa, A., 2017. Economic importance of coralline carbonates. *Rhodolith/Maërl Beds: a global perspective* 87–101.
- Coletti, G., Stainbank, S., Fabbrini, A., Spezzaferri, S., Foubert, A., Kroon, D., Betzler, C., 2018. Biostratigraphy of large benthic foraminifera from Hole U1468A (Maldives): a CT-scan taxonomic approach. *Swiss J. Geosci.* 111, 523–536.
- Coletti, G., Basso, D., Betzler, C., Robertson, A.H.F., Bosio, G., El Kateb, A., Foubert, A., Meilijson, A., Spezzaferri, S., 2019. Environmental evolution and geological significance of the miocene carbonates of the erathostenes seamount (ODP leg 160). *Palaeogeogr. Palaeoclimatol. Palaeoecol.* 530, 217–235.
- Coletti, G., Balmer, E.M., Bialik, O.M., Cannings, T., Kroon, D., Robertson, A.H., Basso, D., 2021. Microfacies evidence for the evolution of Miocene coral-reef environments in Cyprus. *Palaeogeogr. Palaeoclimatol. Palaeoecol.* 584, 110670.
- Coletti, G., Commissario, L., Mariani, L., Bosio, G., Desbailles, F., Soldi, M., Bialik, O.M., 2022. Palaeocene to Miocene southern Tethyan carbonate factories: a meta-analysis of the successions of South-western and Western Central Asia. *The Depositional Record* 8 (3), 1031–1054.
- Condé, V.C., Lana, C.C., Neto, O.C.P., Roesner, E.H., Neto, J.M.M., Dutra, D.C., 2007. Bacia do Ceará. *B. Geoci. PETROBRAS* 15 (2), 347–355.
- Cruz, A.M., Reis, A.T., Suc, J.P., Silva, C.G., Praeg, D., Granjeon, D., Rabineau, M., Popescu, S.M., Gorini, C., 2019. Neogene evolution and demise of the Amapá carbonate platform, Amazon continental margin, Brazil. *Mar. Petrol. Geol.* 105, 185–203. <https://doi.org/10.1016/j.marpetgeo.2019.04.009>.
- D'Almeida, K.S., Souza, M.F.F., Castro, N.O., Vilela, P.C., Leggieri, R.F., Fernandes, R.F., Cardoso, R.A., 2019. Exploratory Potential of the Brazilian Equatorial Margin. Paper presented at the Offshore Technology Conference Brazil, Rio de Janeiro, Brazil, October 2019. <https://doi.org/10.4043/29689-MS>.
- Da Silva, C.P., 2007. Estudo sobre foraminíferos e radiolários do cretáceo, Bacia Pará-Maranhão, margem equatorial brasileira. MSc. Instituto de Geociências, UFPA.
- De Bock, F.J., 1973. Embryonal structures of *Miogypsina*. *Scripta Geol.* 18, 1–15.

- De Mahiques, M.M., Siegle, E., Francini-Filho, R.B., Thompson, F.L., de Rezende, C.E., Gomes, J.D., Asp, N.E., 2019. Insights on the evolution of the living great amazon reef system, equatorial west atlantic. *Sci. Rep.* 9 (1), 13699.
- de Mello e Sousa, S.H., 1994. Estudo microfasciológico da Formação Amapá (Terciário), Bacia da Foz do Amazonas: interpretações bioestratigráficas e paleoecológicas. Tese Doutorado. 2 vol., 309 pp. Inst. Geociência. Universidade de São Paulo, Brasil.
- de Mello e Sousa, S.H., Fairchild, T.R., Tibana, P., 2003. Cenozoic biostratigraphy of larger foraminifera from the Foz do Amazonas Basin, Brasil. *Journal of Micropaleontology* 49, 253–266.
- de Mello e Sousa, S.H., Rossetti, D., Fairchild, T.R., Burone, L., de Mahiques, M.M., Tibana, P., 2009. Microfacies and sequence stratigraphy of the Amapá Formation, late paleocene to early Eocene, Foz do Amazonas Basin, Brazil. *Palaeogeography, Palaeoclimatology, Palaeoecology*. 280, 440–455. <https://doi.org/10.1016/j.palaeo.2009.06.031>.
- Dill, M.A., Vaziri-Moghaddam, H., Seyrafian, A., Behdad, A., Shabafrooz, R., 2020. A review of the Oligo–Miocene larger benthic foraminifera in the Zagros basin, Iran: New insights into biozonation and palaeogeographical maps. *Rev. Micropaleontol.* 66, 100408.
- Field, J.G., Clarke, K.R., Warwick, R.M., 1982. A practical strategy for analyzing multispecies distribution patterns. *Mar. Ecol. Prog. Ser.* 8, 37–52.
- Figueiredo, J., Zalán, P.V., Soares, E.F., 2007. Bacia da Foz do Amazonas. *Bol. Geociências Petrobras* 15, 299–309.
- Geel, T., 2000. Recognition of stratigraphic sequences in carbonate platform and slope deposits: empirical models based on microfacies analysis of Palaeogene deposits in southeastern Spain. *Palaeogeography, Palaeoclimatology, Palaeoecology* 155 (3–4), 211–238. [https://doi.org/10.1016/S0031-0182\(99\)00117-0](https://doi.org/10.1016/S0031-0182(99)00117-0).
- Gomes, B.T., Aguilera, O., da Silva-Caminha, S.A.F., D'Apolito, C., Cárdenas, D., Hocking, E.P., Lemes, K.K.B., 2023. Biostratigraphy and paleoenvironments of the Pirabas Formation (Neogene, Pará state-Brazil). *Mar. Micropaleontol.* 180, 102218.
- Greenop, R., Sosdian, S.M., Henehan, M.J., Wilson, P.A., Lear, C.H., Foster, G.L., 2019. Orbital forcing, ice volume, and CO<sub>2</sub> across the Oligocene-Miocene transition. *Paleoceanogr. Paleoclimatol.* 34 (3), 316–328.
- Griffin, W.J., Powell, J., Pearson, N.J., O'Reilly, S.Y., 2008. Glitter: data reduction software for laser ablation ICP-MS. In: Sylvester, P (Ed.), *Laser ablation ICP-MS in the Earth Sciences: current Practices and Outstanding Issues*. Mineralogi. Agilent Technologies, Vancouver, pp. 308–311.
- Hallock, P., Glenn, E.C., 1986. Larger foraminifera: a tool for paleoenvironmental analysis of Cenozoic carbonate depositional facies. *Palaios* 1, 55–64.
- James, N.P., 1997. In: James, N.P., Clarke, J.A.D. (Eds.), *Cool water carbonates*, 56. SEPM Special Publication, pp. 1–20.
- Kruskal, J.B., 1977. Multidimensional scaling and other methods for discovering structure. In: Enslein, K., Ralston, A., Wilf, H.S. (Eds.), *Statistical Methods for Digital Computers*: 296–339. Wiley, New York.
- Lagabrielle, Y., Goddérís, Y., Donnadieu, Y., Malavieille, J., Suarez, M., 2009. The tectonic history of Drake Passage and its possible impacts on global climate. *Earth Planet Sci. Lett.* 279, 197–211.
- Langer, M.R., Hottinger, L., 2000. Biogeography of selected "larger" foraminifera. *Micropaleontology* 46, 105–126.
- Loeblich Jr., A.R., Tappan, H., 1988. Foraminiferal Genera and their Classification. Van Nostrand Reinhold, Springer, New York, p. 2047pp.
- Michel, J., Borgomano, J., Reijmer, J.J., 2018. Heterozoan carbonates: When, where and why? A synthesis on parameters controlling carbonate production and occurrences. *Earth-Science Reviews* 182, 50–67.
- Miller, K.G., Browning, J.V., Schmelz, W.J., Kopp, R.E., Mountain, G.S., Wright, J.D., 2020. Cenozoic sea-level and cryospheric evolution from deep-sea geochemical and continental margin records. *Sci. Adv.* 6 (20) eaaz1346.
- Mitchell, S.F., Robinson, E., Özcan, E., Jiang, M.M., Robinson, N., 2022. A larger benthic foraminiferal zonation for the Eocene of the Caribbean and central American region. *Carnets Geology* 22 (11), 409–565.
- Murray, J.W., 2006. *Ecology and Applications of Benthic Foraminifera*. Cambridge University Press.
- Nogueira, A.C.R., Amorim, K.B., Góes, A.M., Truckenbrodt, W., Petri, S., Nogueira, A.A. E., Bandeira, J., Soares, J.L., Baía, L.B., Imbiriba, M.J., Bezerra, I.S., Ribas, C.C., Cracraft, J., 2021. Upper oligocene-miocene deposits of Eastern Amazonia: implications for the collapse of Neogene carbonate platforms along the coast of northern Brazil. *Palaeogeogr. Palaeoclimatol. Palaeoecol.*, 110178.
- Özcan, E., Less, G., Baldi-Beke, M., Kollányi, K., Acar, F., 2009. Oligo-Miocene foraminiferal record (Miogypsinidae, Lepidocyclinidae and Nummulitidae) from the Western Taurides (SW Turkey): biometry and implications for the regional geology. *J. Asian Earth Sci.* 34 (6), 740–760.
- Pamplona, H.R.P., 1969. Litoestratigrafia da Bacia Cretácea de Barreirinhas. *Rio de Janeiro. Bol. Tec. Petrobras* 12 (3), 261–290.
- Pellegrini, B.S., Ribeiro, H.J.P.S., 2018. Exploratory plays of Pará-Maranhão and Barreirinhas basins in deep and ultra-deep waters, Brazilian Equatorial Margin. *Braz. J. Geology* 48 (3), 485–502. <https://doi.org/10.1590/2317-4889201820180146>.
- Perrin, C., 1992. Signification écologique des foraminifères acervulinidés et leur rôle dans la formation de faciès récifaux et organogènes depuis le Paléocène. *Geobios* 25 (6), 725–751.
- Perrin, C., Bosellini, F.R., 2012. Paleobiogeography of scleractinian reef corals: changing patterns during the Oligocene–Miocene climatic transition in the Mediterranean. *Earth Sci. Rev.* 111 (1–2), 1–24.
- Pessoa Neto, O.C., Soares, U.M., Silva, J.G.F., Roesner, E.H., Florencio, C.P., Souza, C.A. V., 2007. Bacia Potiguar. *Boletim de Geociências da PETROBRAS* 15 (2), 357–369.
- Pomar, L., 2001. Types of carbonate platforms: a genetic approach. *Basin Res.* 13 (3), 313–334.
- Pomar, L., Baceta, J.I., Hallock, P., Mateu-Vicens, G., Basso, D., 2017. Reef building and carbonate production modes in the west-central Tethys during the Cenozoic. *Mar. Petrol. Geol.* 83, 261–304.
- Renema, W., 2018. Terrestrial influence as a key driver of spatial variability in large benthic foraminiferal assemblage composition in the Central Indo-Pacific. *Earth Sci. Rev.* 177, 514–544.
- Roberts, N.M., Drost, K., Horstwood, M.S., Condon, D.J., Chew, D., Drake, H., Milodowski, A.E., McLean, N.M., Smye, A.J., Walker, R.J., Haslam, R., Hodson, K., Imber, J., Beaudoin, N., Lee, J.K., 2020. Laser ablation inductively coupled plasma mass spectrometry (LA-ICP-MS) U–Pb carbonate geochronology: strategies, progress, and limitations. *Geochronology* 2 (1), 33–61.
- Roberts, N.M., Rasbury, E.T., Parrish, R.R., Smith, C.J., Horstwood, M.S., Condon, D.J., 2017. A calcite reference material for LA-ICP-MS U–Pb geochronology. *Geochemistry, Geophysics, Geosystems* 18 (7), 2807–2814.
- Robinson, E., 2004. Zoning the White Limestone Group of Jamaica using larger foraminiferal genera: a review and proposal. *Cainozoic Res.* 3 (1/2), 39–75.
- Sanei, H., Ardakani, O.H., Akai, T., Akihisa, K., Jiang, C., Wood, J.M., 2020. Core versus cuttings samples for geochemical and petrophysical analysis of unconventional reservoir rocks. *Sci. Rep.* 10 (1), 7920.
- Schaller, H., Vasconcelos, D.N., Castro, C.C., 1971. Estratigrafia preliminar da bacia sedimentar da Foz do Amazonas. In: An. 25º Congresso Brasileiro de Geologia. SBG., São Paulo, pp. 189–202, 3.
- Soares, E.F., Zalán, P.V., Figueiredo, J.-J.P., Trosdorf Jr, I., 2007. Bacia do pará-maranhão. *Bol. Geociências Petrobras* 15, 321–330.
- Testa, V., Bosence, D.W., 1999. Physical and biological controls on the formation of carbonate and siliciclastic bedforms on the north-east Brazilian shelf. *Sedimentology* 46 (2), 279–301.
- Trosdorf Jr., I., Zalán, P.V., Figueiredo, J.J.P., Soares, E.F., 2007. Bacia de Barreirinhas. *Bol. Geociências Petrobras* 15, 331–339.
- Van Vesse, E.J., 1978. Study of lepidocyclinidae from south-East Asia, particularly from java and borneo. *Utrecht Micropalaeontological Bulletin* 19, 1–163.
- Vermeesch, P., 2021. IsoplotR: A free and open toolbox for geochronology. *Geoscience Frontiers* 12 (5), e101227. <https://doi.org/10.1016/j.gsf.2018.04.001>.
- Zachos, J., Pagani, M., Sloan, L., Thomas, E., Billups, K., 2001. Trends, rhythms, and aberrations in global climate 65 Ma to present. *Science* 292 (5517), 686–693.
- Zalán, P.V., 2015. Re-interpretation of an Ultra-deep Seismic Section in the Pará-Maranhão Basin - Implications for the Petroleum Potential of the Ultra-deep Waters. Offshore Technical Conference, Brazil. OTC-26134-MS.
- Zalán, P.V., Hodgson, N., Saunders, M., 2019. Foz Do Amazonas and Pará-Maranhão Basins Ready to Replicate Guyana Success. AAPG Annual Convention and Exhibition, San Antonio, Texas, 30624. Search and Discovery Article.